Images were acquired by a confocal laser microscope A1. Data were analyzed using ImagePro Plus 4.5.1 (Roper).

Mass spectrometry

Mass Spectrometry analysis was performed according to the procedure described in supplemental Methods.

In vivo analysis for retinal angiogenesis

Mice were treated according to the guidelines of Ehime University. This procedure was modified from a published procedure.[4] Generation of *BAZF* knockout mice was reported previously.[22] For the assessment of retinal angiogenesis in $BAZF^{+/+}$ and $BAZF^{-/-}$ littermate mice, the retinas were analyzed at P5. Eyes were fixed in 4% PFA overnight at 4°C. For single staining, retinas were incubated in PBlec buffer (1% Triton X-100, 1mM $CaCl_2$, 1mM $MgCl_2$, and 1mM $MnCl_2$ in PBS (pH 6.8) containing 10% FCS for 1 hour. The retinas were incubated overnight in PBlec buffer containing isolectin B4–Alexa Fluor 647 (Invitrogen). Image was obtained by a confocal laser microscopy A1. Quantification of diameter of vascular area, isolectin $B4^+$ area, branch points, and numbers of filopodia was performed with ImagePro Plus.

Angiogenesis analysis in wound healing

Wound healing experiments were performed in $BAZF^{+/+}$ (n = 13) and $BAZF^{-/-}$ (n = 13) littermate mice according to a published procedure.[23] The wounded skin tissues were fixed with 10% formalin in phosphate buffer (pH 7.2) and embedded in paraffin. The sections were stained with hematoxylin and eosin. For anti-CD31 staining, the sections were autoclaved in 20mM citrate buffer (pH 6.0) for 20 minutes at 121°C, and the sections were stained with an anti-CD31 antibody (clone: SZ31, Dianova). Sections were further reacted with an anti–rat IgG-HRP antibody, and visualized by a DAB substrate kit (Vector). $CD31^+$ area, avascular area and leading edge ratio were measured by ImagePro Plus 4.5.1.

Statistical analysis

Data are based on a minimum of 3 independent experiments, or 3 mutant or control animals for each stage. The results are represented as mean ± SE. The 2 groups were compared using the student *t* test. ANOVA with Bonferroni posthoc test was used for multiple comparisons. $P < .05$ was considered statistically significant.

Further information is also described in supplemental Methods.

Results

VEGF-A up-regulates *BAZF* in HUVEC

Down-regulation of Notch signaling by knockdown of the related molecules or a treatment of γ-secretase inhibitor increased sensitivity to VEGF-A stimulation in endothelial network formation (supplemental Figure 1A-C). As shown in supplemental Figure 1D, *Hairy/enhancer-of-split related with YRPW motif protein 1* (*HEY1*) and *HEY2*, target genes of Notch signaling, were also significantly down-regulated as an early response of VEGF-A stimulation. Therefore, we hypothesized that angiogenesis sprouting might require transient disconnection of Notch signaling. To characterize genes up-regulated by VEGF-A stimulation, we compared the gene expression profiles of control and VEGF-A–treated HUVECs using a DNA microarray representing 458 of the C2H2 ZnF transcriptional repressor genes, resulting in the identification of *BAZF* as being up-regulated in response to VEGF-A exposure (supplemental Figure 1E). Quantitative RT-PCR and Western blotting confirmed that *BAZF* was transiently induced at the level of both mRNA (maximum induction approximately 2- to 2.5-fold) and protein (maximum induction approximately 3-fold) in HUVECs (Figure 1A-B). *BAZF* mRNA was up-regulated after 2 hours of VEGF-A stimulation and rapidly returned to the basal level (Figure 1A), and BAZF protein increased up to 4 hours before gradually decreasing to the basal level at 12 hours (Figure 1B). Interestingly, BCL6, known as a hetero-binding partner of BAZF,[24] was undetectable at the mRNA level and had no response to VEGF-A stimulation in HUVECs (supplemental Figure 1E). These results demonstrate that *BAZF* is a target of VEGFR signal transduction in HUVECs.

BAZF regulates network formation of HUVECs in vitro

To determine the effect of BAZF overexpression, HUVECs were infected with a BAZF-encoding adenovirus (AdBAZF). AdBAZF-infected HUVECs exhibited filopodia protrusion without VEGF-A stimulation on the Matrigel in a dose-dependent manner up to a multiplicity of infection (MOI) of 250 (supplemental Figure 1F-G). Further, we performed a HUVEC fibrin gel bead assay to examine the effect of BAZF on EC sprouting. As shown in Figure 1C, much abundant filopodia protrusion was induced from AdBAZF-infected HUVECs than GFP-encoding adenovirus (AdGFP)–infected HUVECs (27 vs 9 cells with filopodia formation on 50 beads).

To confirm endogenous BAZF function in HUVEC, we knocked down the level of the *BAZF* mRNA by siRNA transfection of cells. BAZF siRNA reduced not only the *BAZF* mRNA by more than 80% (supplemental Figure 2A), but the BAZF protein as well (Figure 1D). VEGF-A–induced EC network formation was completely abrogated by BAZF siRNA (Figure 1E-G). However, *BAZF* knockdown had no effect on cell adhesion and spreading on the Matrigel (supplemental Figure 2B-C). Time-lapse image analysis also showed that there was no difference in the mobility and the incidence of cell-cell contact for the control and BAZF siRNA-transfected HUVECs (data not shown). In addition, we used BAZF siRNA transfection to examine the role of BAZF on network formation by different type of ECs, including human coronary artery, dermal microvascular, and retinal ECs in culture. *BAZF* knockdown completely abrogated the network formation in these EC cultures despite the presence of VEGF-A (supplemental Figure 2D-E). These results suggest that under certain conditions, BAZF might play a crucial role for EC filopodia protrusion, elongation, and network formation.

Inhibition of Notch signaling rescues the disruption of EC network formation by *BAZF* knockdown

If BAZF indeed plays a role in VEGFR cross-talk with Notch signaling, we hypothesized that blockade of Notch signaling would rescue the disruption of EC network formation by BAZF siRNA. Treatment of BAZF siRNA-transfected HUVEC cultures with the γ-secretase inhibitor DAPT resulted in the recovery of VEGF-A–induced network formation (Figure 2A-B). Similar to the effects of DAPT, *Notch1*, or *CBF1* knockdown also rescued the disruption of EC network formation by BAZF siRNA (Figure 2A-B). In addition, the levels of the *HEY1* and *HEY2* mRNAs increased more than 2-fold in *BAZF* knocked down HUVECs. On the other hand, the level of *VEGFR2* mRNA, one of down-regulating target genes of Notch signaling,[25,26] decreased in BAZF knocked down HUVEC (Figure 2C). In contrast, BAZF-overexpressing HUVECs by AdBAZF infection significantly reduced the levels of *HEY1* and *HEY2* transcripts (Figure 2D). These data suggest that BAZF modulates the Notch signaling pathway as a negative regulator to promote angiogenesis by VEGF-A.

The ZnF domain of BAZF interacts with the amino terminal region of CBF1

To determine whether there is a physical interaction between BAZF and CBF1, we performed an assay of immunoprecipitation Western

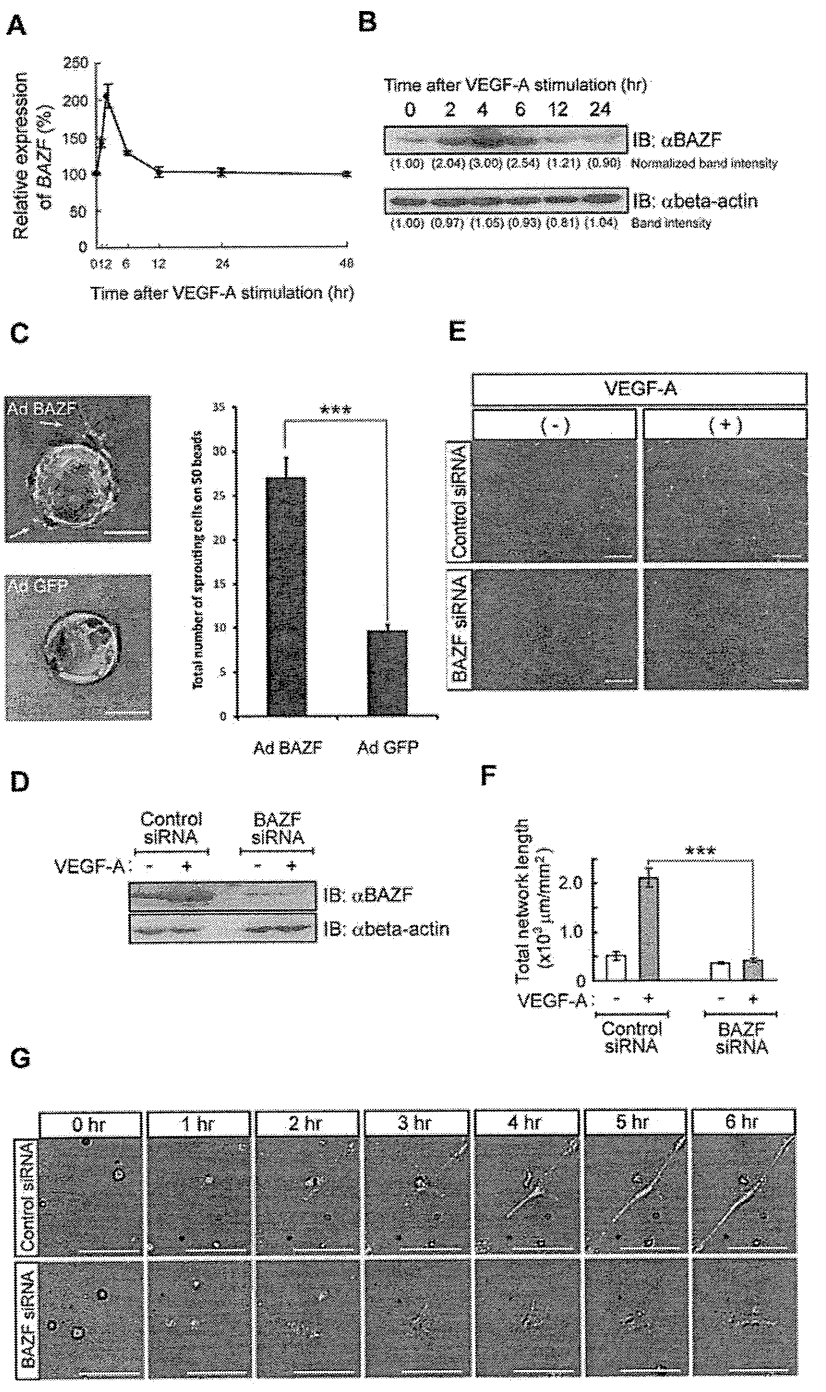

Figure 1. BAZF regulates EC network formation in culture. (A) Expression pattern of *BAZF* mRNA after VEGF-A (50 ng/mL) stimulation in HUVECs. Quantitative RT-PCR of *BAZF* mRNA was performed using a TaqMan gene expression system. The results represent mean values from 3 independent experiments. Error bars represent ± SD. (B) Analysis of BAZF protein level in HUVECs after VEGF-A stimulation by Western blotting using an anti-BAZF antibody. Relative intensity of each band was measured by Lane Analyzer 3.0 software (ATTO) and normalized relative to β-actin (loading control). (C) Angiogenic sprouting from AdBAZF-infected or AdGFP-infected HUVECs. Arrows show sprouting cells. Left panels represent microscopic images, and right panel shows total number of sprouting cells in 50 beads. Scale bar: 100 μm (***$P < .001$). (D) Protein level of BAZF in HUVEC transfected with *BAZF* or control siRNA with or without VEGF-A stimulation. BAZF protein was detected by Western blotting using an anti-BAZF antibody. (E) *BAZF* knockdown disrupts VEGF-A–induced network formation of HUVECs on the Matrigel. The cells were stained with Calcein-AM and the images were acquired. Scale bar: 500 μm. (F) Quantification of the network formation of HUVEC transfected with *BAZF* or control siRNA. The total length of the network per field (mm²) was measured by ImagePro Plus software 4.5. (Roper). The results represent mean values from 3 experiments. Error bars represent ± SD (***$P < .001$). (G) Time-lapse imaging of the network formation in HUVEC treated with *BAZF* or control siRNA. Scale bar: 10 μm.

blotting between BAZF and CBF1 in HUVEC, resulting in the successful detection of endogenous BAZF coimmunoprecipitated with CBF1 in HUVEC in a VEGF-A–dependent fashion (Figure 2E). To analyze more precisely the interaction between BAZF and CBF1, we performed glutathione S-transferase (GST) pull-down assays. We constructed various V5-tagged deletion mutants for both BAZF and CBF1 (supplemental Figure 3D-F), which were then expressed in HT1080 cells. A GST-CBF1 or a GST-BAZF fusion protein was used to capture the various V5-tagged mutants from HT1080 cell extracts, and the captured proteins were analyzed by Western blotting using an anti-V5 antibody (supplemental Figure 3A-F). The results showed that the N-terminal region (residues 1-178 aa) corresponding to the LAG1-DNA binding region, but not the center or the C-terminal region of CBF1, bound the ZnF domain of BAZF (Figure 2F). These results suggested that BAZF might interfere with Notch signaling by competing with the intracellular domain of Notch (NICD) for binding to CBF1. To test this hypothesis, we analyzed the effect of overexpressing V5-tagged BAZF (V5-BAZF) on the ability of Myc-tagged Notch1 ICD (Myc-N1ICD) to be coimmunoprecipitated with FLAG-tagged CBF1 (FLAG-CBF1). As shown in supplemental Figure 3G, the overexpression of V5-BAZF did not interfere with the FLAG-CBF1-Myc-N1ICD interaction, consistent with the fact that BAZF and NICD bind to different regions of CBF1.[27] BAZF

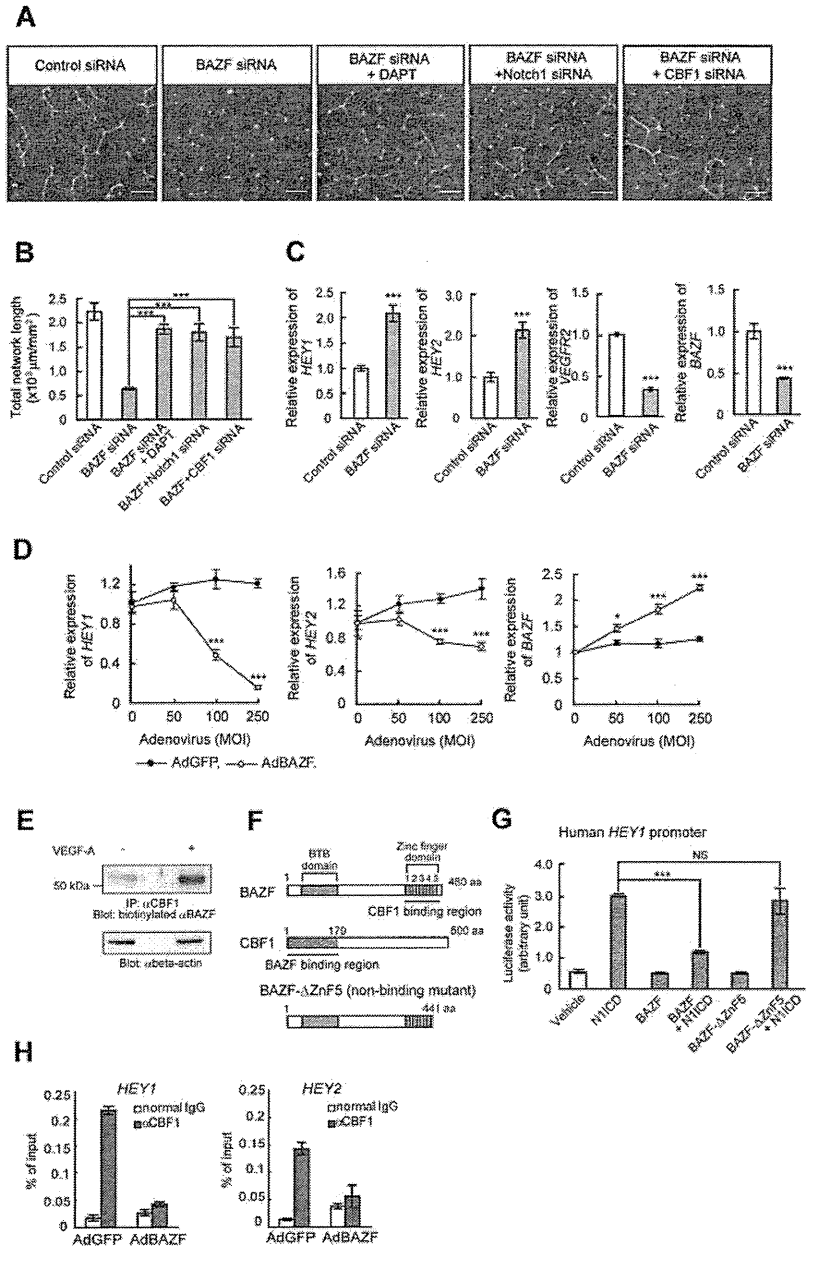

Figure 2. BAZF down-regulates Notch signaling by targeting CBF1. (A-B) Disruption of network formation by *BAZF* knockdown was rescued by DAPT, *Notch1* siRNA, or *CBF1* siRNA. (A) HUVECs were transfected with indicated combinations with siRNAs and DAPT. After the transfection and serum-starvation, the cells were seeded on the Matrigel with or without DAPT (1 μM) in the presence of VEGF-A. Scale bar: 100 μm. (B) Total network length per mm² was quantified by ImagePro Plus. The results represent mean values from 3 experiments. Error bars represent ± SD. (C) *BAZF* knockdown increases the expression of Notch target genes, *HEY1* and *HEY2*. The expression levels of the *HEY1*, *HEY2*, *VEGFR2*, and *BAZF* mRNAs were analyzed by quantitative RT-PCR. (D) BAZF overexpression down-regulates *HEY1* and *HEY2* expression. The expression levels of *HEY1* and *HEY2* mRNAs were analyzed by quantitative RT-PCR (*$P < .05$, ***$P < .001$). (E) Interaction of BAZF with CBF1. The cell lysates were prepared from VEGF-A–treated (6 hours) or non-treated HUVECs and immunoprecipitated with an anti-CBF1 antibody. The immunoprecipitates were analyzed by Western blotting with a biotinylated anti-BAZF antibody. Beta-actin was detected as a loading control. (F) A molecular schema of BAZF-CBF1 interaction designed by the data in supplemental Figure 3. BAZF-ΔZnF5 is a mutant lacking CBF1-binding capacity. (G) A reporter assay of *HEY1* promoter activity. HUVECs were cotransfected with a luciferase reporter plasmid containing human *HEY1* promoter, along with the plasmids encoding N1ICD, BAZF, and/or BAZF-ΔZnF5. Luciferase activities are represented as arbitrary units. Error bars show ± SD of 5 samples from 3 independent experiments (***$P < .001$). NS indicates not significant. (H) A ChIP assay using an anti-CBF1 antibody in HUVECs infected with AdBAZF or AdGFP. The CBF1 binding element on human *HEY1* and *HEY2* promoters was detected in the immunoprecipitates by quantitative RT-PCR.

knockdown had no major effects on N1ICD production (supplemental Figure 3H).

We next examined the functional consequences of the interaction between BAZF and CBF1 using a luciferase reporter assay (Figure 2G). For this assay, HUVEC were transfected with a reporter plasmid in which expression of luciferase was controlled by the human *HEY1* promoter. Luciferase activity increased under enforced coexpression of N1ICD. The luciferase activity induction by N1ICD was blocked if BAZF was also overexpressed; however, overexpression of the nonCBF1-binding mutant, BAZF-ΔZnF5 (Figure 2F) had no effect on N1ICD-induced reporter activation, suggesting that BAZF suppressed Notch signaling by regulation of CBF1 transcriptional activity (Figure 2G). To investigate the mechanism of the transcriptional repression by BAZF, we performed a ChIP assay in HUVECs using an anti-CBF1 antibody to determine the relative extent to which the *HEY1* and *HEY2* promoter regions were bound to CBF1. CBF1 binding on the *HEY1* or *HEY2* promoters was clearly detected in control HUVECs that had been infected with AdGFP. However, BAZF overexpression dramatically abrogated the CBF1 binding on these promoter regions (Figure 2H). These data indicate that BAZF suppresses the transcriptional activation in response to Notch signaling by releasing CBF1 from the targeted gene promoter regions.

Up-regulation of BAZF leads to degradation of CBF1 via recruitment of cullin3

We noticed that the immunostaining intensity of endogenous CBF1 got weaker in a time-dependent manner in HUVECs after VEGF stimulation or BAZF, but not BAZF-ΔZnF5 overexpression (Figure 3A-B), whereas the level of *CBF1* mRNA was constant on a BAZF-overexpressing condition (supplemental Figure 3I).

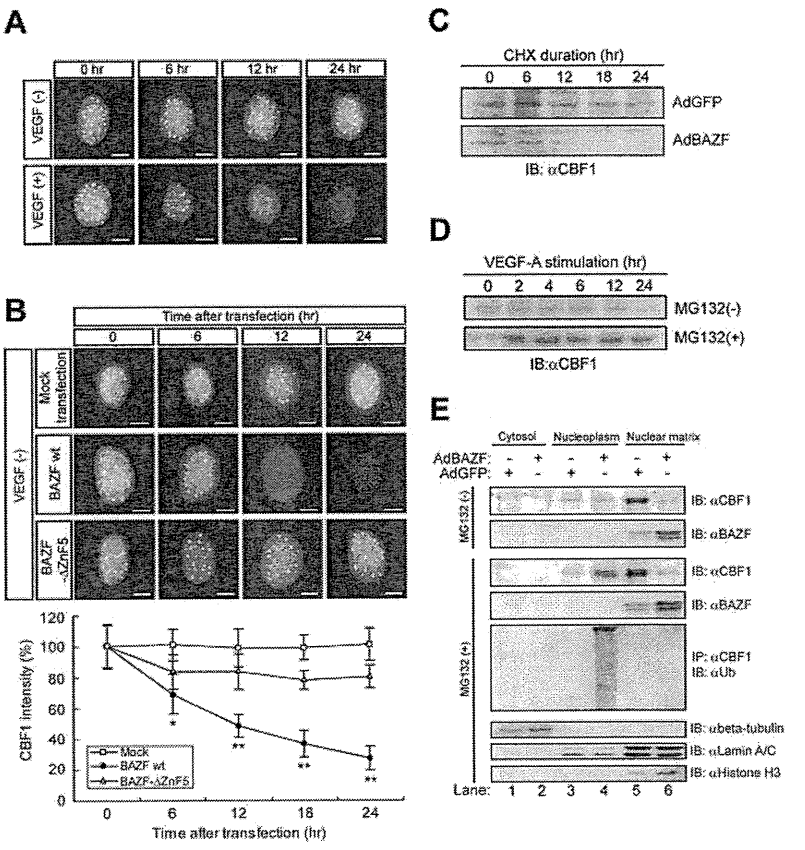

Figure 3. BAZF regulates polyubiquitination and degradation of CBF1. (A-B) Immunocytostaining of endogenous CBF1 in HUVECs with and without VEGF-A. Scale bar: 5 μm. (A) HUVECs were treated with VEGF-A for indicated hours and stained with anti-CBF1. (B) HUVECs were transfected with Mock, BAZF wild-type (WT), or BAZF-ΔZnF5. After transfection, the cells were stained with anti-CBF1. The images were acquired by ImageXpress Micro (Molecular Devices). The signal intensity of CBF1 staining in a hundred cells was measured by ImagePro Plus. Error bars show ± SD of independent triplicates (*$P < .05$, **$P < .01$). (C-D) Turnover of CBF1 in HUVECs. (C) After HUVEC were infected with AdBAZF or AdGFP, CHX was added to cell cultures at a concentration of 10μM. Cells were lysed at indicated hours post-CHX addition. Endogenous CBF1 in the chromatin-enriched nuclear matrix fraction was detected by Western blotting with an anti-CBF1 antibody. (D) HUVECs were treated with VEGF-A for indicated hours in the presence or absence of MG132. (E) Western blotting of CBF1 and BAZF in cytosol, nucleoplasm (soluble factions), and chromatin-enriched nuclear matrix (insoluble fraction) of AdBAZF or AdGFP infected HUVECs in the presence or absence of MG132. After infection and treatment of MG132, the cells were then harvested and fractionated to cytosol, nucleoplasm, and chromatin-enriched nuclear matrix fractions according to the protocol described in supplemental Methods. CBF1 and BAZF were detected by Western blotting with antibodies against each protein. Immunoprecipitation was performed using an anti-CBF1 antibody. Ubiquitinated CBF1 was detected by probing Western blots of the precipitates with an anti-ubiquitin antibody. Beta-tubulin, lamin A/C, and histone H3 were detected as fraction markers.

Next, we examined CBF1 protein stability in the cell lysates collected from cultures in which new translation was blocked by the presence of cycloheximide (CHX). Western blotting examinations showed that CBF1 protein rapidly disappeared with a half-life of approximately 12 hours in cells infected with AdBAZF, although it was constant (up to 24 hours) after AdGFP infection (Figure 3C). Therefore, we further analyzed whether the disappearance of CBF1 depends on protein degradation or not by Western blotting of cell lysates with a treatment of a proteasome inhibitor MG132. The level of CBF1 protein apparently increased (Figure 3D). Next, we fractionated cell lysates into cytosol, nucleoplasm, and chromatin-enriched nuclear matrix (nuclear matrix) fractions, and performed Western blotting to detect CBF1 (Figure 3E). In the absence of MG132, whereas CBF1 was dominantly detected in the nuclear matrix (Figure 3E top panel, lane 5), the level of CBF1 dramatically decreased in the nuclear matrix after AdBAZF infection (Figure 3E top panel, compare lanes 5-6). However, addition of MG132 restored CBF1 protein stability in the nucleoplasm in AdBAZF-infected cells (Figure 3E third panel, lane 4). Given the results, we next analyzed polyubiquitination of endogenous CBF1 by immunoprecipitation Western blotting (Figure 3E 5th panel). Polyubiquitinated CBF1 was only detected in the nucleoplasm, when AdBAZF, but not the AdGFP, was infected in HUVECs (Figure 3E 5th panel, compare lanes 3-4). On the other hand, BAZF was primarily detected in the nuclear matrix (Figure 3E 2nd and 4th panels, lanes 5-6), but was essentially undetectable in the cytosol or the nucleoplasm (Figure 3E 2nd and 4th panels, lanes 1-4) in the presence or absence of MG132 regardless of whether the cells were infected with AdBAZF. These data strongly suggest that BAZF, when overexpressed, triggered CBF1 polyubiquitination as well as subcellular translocalization from the nuclear matrix fraction to the nucleoplasmic fraction and proteasome-dependent degradation. It is important to note that the level of overexpression achieved with AdBAZF infection (2- to 3-fold over the basal level) was similar to the level of induction accomplished by VEGF-A stimulation.

BTB domains can interact with cullin3 (CUL3), a main component of the CUL3-based E3 ubiquitin ligase complex.[28-32] To examine the possible interaction between CUL3 and BTB domain of BAZF, we performed immunoprecipitation and Western blotting using BAZF deletion mutants, and revealed that CUL3 interacted primarily with the BTB-center domain and faintly with the ZnF domain of BAZF (supplemental Figure 4A-B). Then, we performed a simultaneous immunostaining analysis of endogenous CUL3 and CBF1 in BAZF siRNA or control siRNA-treated HUVEC under conditions of VEGF-A stimulation. Under control siRNA-treatment, CUL3 and CBF1 distributed throughout the nucleus in the absence of VEGF-A stimulation. However, VEGF-A addition dramatically triggered their colocalization with ring shape at the PML nuclear body after 6 hours of incubation (supplemental Figure 4A-C). In contrast, under BAZF siRNA-treatment, the both localization was neither altered nor merged after 6 hours of incubation with VEGF-A (Figure 4A). We also analyzed CUL3-CBF1 complex formation by a combination assay of immunoprecipitation and multiple reaction monitoring (MRM) analysis by mass spectrometry (MS). Based on tandem MS information obtained from tryptic digests of recombinant CUL3 protein, we selected Q1 (precursor)/Q3(fragment) ion pairs for 3 peptides (NAIQEIQR, EDGSEVGVGGAQVTGSNTR and FLLESFNNDR; supplemental Figure 5A-C), and measured recombinant CUL3

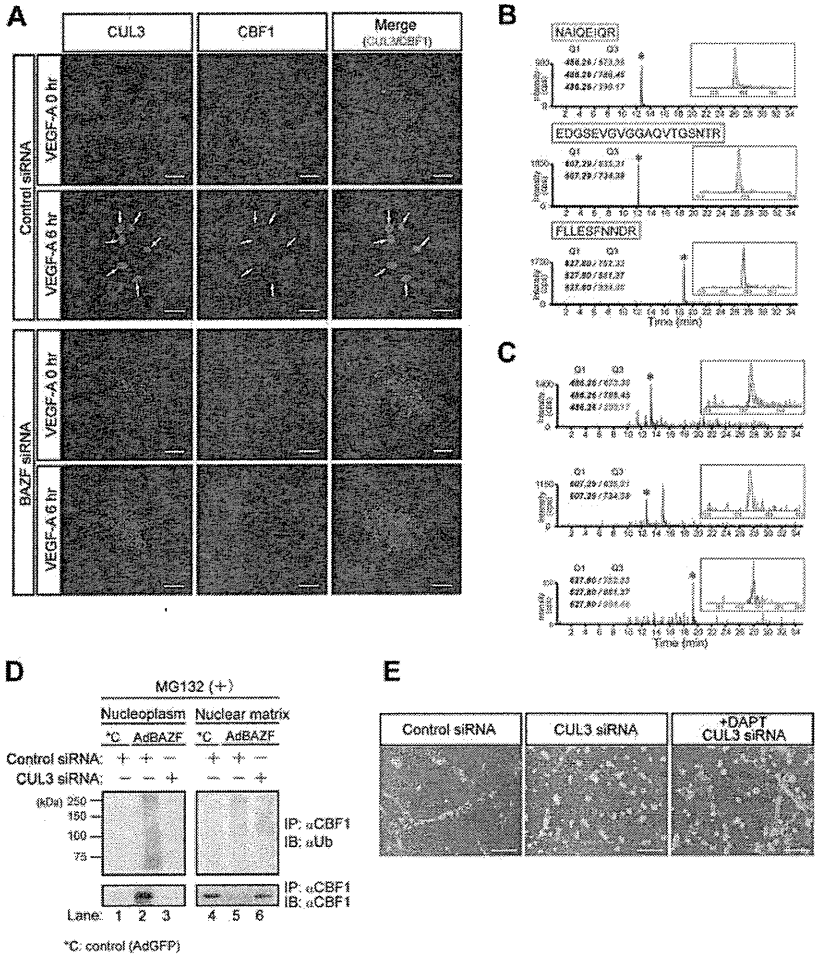

Figure 4. CUL3 mediates BAZF-induced degradation of CBF1. (A) Super-resolution imaging of colocalization of endogenous CUL3 and CBF1 on VEGF-A–induced ring structures. HUVEC were transfected with BAZF or control siRNA. After transfection and serum starvation, the cells were stimulated with VEGF-A for 6 hours. The cells were immunostained with anti-CUL3 (green) and anti-CBF1 (red) antibodies. The images were acquired by a structured illumination microscopy N-SIM (Nikon) to analyze colocalization of endogenous CUL3 and CBF1. Arrows: VEGF-A–induced ring structures including CUL3 and CBF1. Scale bar: 5 μm. (B-C) MRM analysis of CUL3 using hybrid triple quadrupole/linear ion trap mass spectrometer. (B) Representative MRM profiles of in-gel tryptic peptides from recombinant CUL3. Gel-separated CUL3 tryptic peptides in supplemental Figure 5 were subjected to MRM analysis. * indicates detected CUL3 ion peaks (enlarged view shown in the inset). MRM transitions for the targeted CUL3 peptides were as follows: NAIQEIQR (m/z 486.26→673.36, 786.45, and 299.17), EDGSEVGVGGAQVTGSNTR (m/z 607.29→635.31, and 734.38), and FLLESFNNDR (m/z 627.80→752.33, 881.37, and 994.46). (C) MRM analysis of endogenous CUL3 coimmunoprecipitated with CBF1. Tryptic digests of the immunoprecipitates were subjected to MRM analysis. * indicates Ion peaks assigned to the CUL3 peptide (an enlarged view is shown in the inset). CBF1 was also detected from immunoprecipitates by MRM analysis (data not shown). (D) Effect of *CUL3* knockdown on polyubiquitination and degradation of CBF1 induced by AdBAZF infection. HUVECs were transfected with *CUL3* siRNA or control siRNA. After transfection, HUVECs were infected with AdBAZF or AdGFP. And then, MG132 was added to the cell culture (50μM). The cells were harvested and fractionated into nucleoplasm and chromatin-enriched nuclear matrix fractions. Immunoprecipitation was performed using an anti-CBF1 antibody. Polyubiquitinated or nonpolyubiquitinated CBF1 was detected using anti-ubiquitin and anti-CBF1 antibodies. (E) Network formation of *CUL3* knocked down HUVECs in the presence or absence of DAPT. HUVECs were transfected with CUL3 siRNA or control siRNA. The cells were seeded on the Matrigel with VEGF-A with or without DAPT. Twelve hours later, the images were acquired by a microscope. Scale bar: 20 μm.

(Figure 4B) and the immunoprecipitates by an anti-CBF1 antibody (Figure 4C) in MRM mode. Three Q1/Q3 ion pairs were clearly detected in the immunoprecipitates as well as recombinant CUL3, which indicates that an anti-CBF1 antibody coprecipitated CUL3. Taken together, these data indicate that BAZF can mediate a trimer complex formation with CUL3 and CBF1.

To explore the functional consequences of the interaction between BAZF and CUL3, we performed *CUL3* knockdown using a CUL3-specific siRNA (supplemental Figure 4D). Polyubiquitination of endogenous CBF1 in HUVEC infected with AdBAZF or AdGFP was analyzed in the presence or absence of CUL3 siRNA with a treatment of MG132 (Figure 4D). Polyubiquitinated CBF1 was mainly detected in the nucleoplasm (Figure 4D lane 2) in the AdBAZF-infected HUVECs. However, the polyubiquitination of CBF1 in the nucleoplasm was completely abrogated by *CUL3* knockdown (Figure 4D lane 3). CBF1 protein primarily existed in the nuclear matrix (Figure 4D compare lanes 1-4) in the AdGFP-infected HUVEC. AdBAZF-infection altered the subcellular localization of CBF1 from the nuclear matrix to the nucleoplasm (Figure 4D lanes 2 vs 5), which was also completely abrogated by *CUL3* knockdown (Figure 4D lanes 3 vs 6).

We next investigated the role of CUL3 in VEGF-A–induced HUVEC network formation on the Matrigel. When the cells were transfected with CUL3 siRNA before plating on the Matrigel, VEGF-A failed to induce network formation. Network formation was partially restored by the addition of DAPT to the cultures (Figure 4E).

Taken together, these results strongly suggest that in angiogenic response to VEGF-A stimulation, BAZF makes a complex with CUL3 and CBF1 at the PML nuclear body, which triggers CUL3-dependent CBF1 polyubiquitination, subcellular translocalization, and degradation.

BAZF$^{-/-}$ mice show angiogenic retardation and up-regulation of Notch signaling in the developing retina

It has been reported that *BAZF*$^{-/-}$ mice are viable, healthy, and normal in size.[22,33] Vasculogenesis and angiogenesis abnormalities in *BAZF*$^{-/-}$ mice have not been reported. However, close examination of the retinas of mice with gene disruption of *BAZF* showed reduction in vascular density and sprouts in the peripheral part of the developing retinal vascular plexus at P5 (Figure 5A-E, supplemental Figure 6A). A tissue immunostaining assay with an anti-BAZF antibody revealed that BAZF was expressed in the developing retinal vascular plexus in *BAZF*$^{+/+}$ mice (Figure 5F). Immunostaining of CBF1 and HEY1 revealed that their protein levels markedly up-regulated in the retinas of *BAZF*$^{-/-}$ mice (Figure 5G-I). It was similar to a phenotype identical to that reported for the ECs of the retinas in mice with an excessively active Notch signaling.[2] On the contrary, inhibition of Notch signal

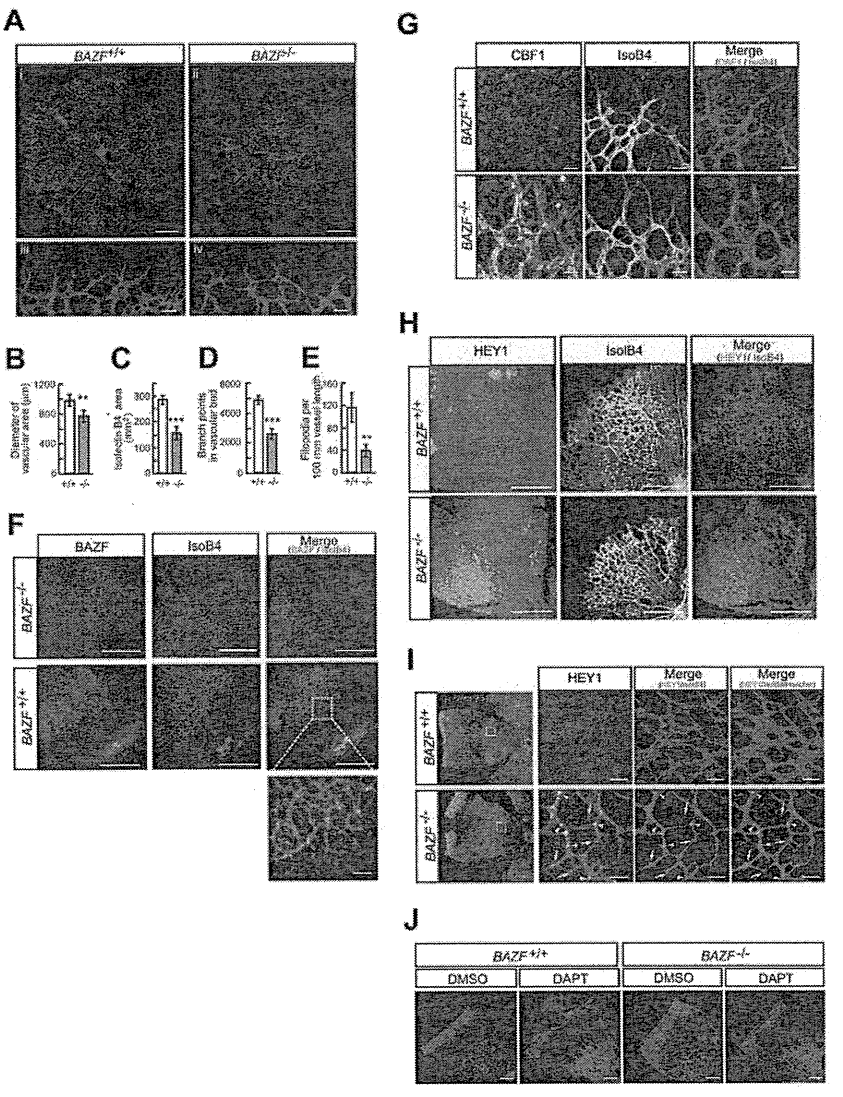

Figure 5. Up-regulation of Notch signaling and angiogenic suppression in BAZF knockout mouse retina. Littermate mice of representing 2 genotypes (*BAZF*$^{+/+}$ and *BAZF*$^{-/-}$) were assessed for retinal angiogenesis and Notch signaling at P5. The retinas were stained with isolectin B4, and then flat-mounted for confocal laser microscopic analysis. (A) Whole retinal vascular bed (i and ii, scale bar: 200 μm) and front (iii and iv, scale bar: 20 μm) of *BAZF*$^{+/+}$ and *BAZF*$^{-/-}$ mice. Quantitative analyses of the diameter of the vascular area (B), isolectin B4^{+} area (C), branching points (D), and the number of filopodia (E) in *BAZF*$^{+/+}$ (n = 9) and *BAZF*$^{-/-}$ (n = 3) retinas. Error bars represent ± SD (**$P < .01$, ***$P < .001$). (F) BAZF immunostaining in whole-mount retina. Both *BAZF*$^{+/+}$ and *BAZF*$^{-/-}$ retinas were stained with isolectin B4 and anti-BAZF. Scale Bar: 500 μm (50 μm in the enlarged image). (G) CBF1 immunostaining in whole-mount retina. Retinas were stained with isolectin B4 and anti-CBF1 or normal rabbit IgG as a negative control. Scale bar: 15 μm. (H) HEY1 immunostaining in whole-mount retinal vasculature. Retinas were stained with isolectin B4 and anti-HEY1 antibody. Scale bar: 200 μm. (I) HEY1 localization in retinal vascular plexus. Nuclear localization (arrowheads) of HEY1 in stalk ECs, whereas faint signals in sprouting tip cells (arrows). Endothelia were also stained with isolectin B4. Scale bar: 20 μm. (J) Formation of hyperfused plexus by Notch signal inhibition in retinas. After administration of DMSO or DAPT (100 mg/kg) at P3 and P4, retinas were collected at P5. Retinas were stained with isolectin B4 and Hoechst33342. Images were obtained by a confocal laser microscopy. Scale bar: 200 μm.

by injection of DAPT into *BAZF*$^{-/-}$ and *BAZF*$^{+/+}$ retinas resulted in the formation of hyperfused plexus similarly (Figure 5J). Taken together, these findings suggest that endogenous BAZF regulates angiogenesis by inactivating Notch signaling during development of the mouse retina.

BAZF$^{-/-}$ mice show the impaired angiogenesis in skin wound healing

Because it is well known that wounded tissues require angiogenesis for repair, we analyzed skin wound healing in *BAZF*$^{-/-}$ mice. H&E staining of wounded skin section of *BAZF*$^{-/-}$ mice at day 7 revealed the impairment of healing (Figure 6A and C). Immunostaining of CD31 in the section showed that CD31 positive vascular area in wound sites, especially in granulation sites of *BAZF*$^{-/-}$ mice was much smaller than that of *BAZF*$^{+/+}$ mice (Figure 6B-E), and that the larger avascular area was necrotic tissue in *BAZF*$^{-/-}$ mice (Figure 6C and F). In consequence, delayed wound healing in *BAZF*$^{-/-}$ mice was observed with statistically significant at 3 and 7 days after wounding (supplemental Figure 6B-D). These data suggest that wound-induced angiogenic response was impaired in *BAZF*$^{-/-}$ mice, resulting in the delay of wound healing.

Discussion

BAZF is a protein most closely related to BCL6, and has BTB and ZnF domains in the N and the C-terminal regions, respectively.[24] It has been suggested that BAZF and BCL6 bind an identical DNA sequence similar to a Stat binding motif,[24,34,35] and that BAZF functions as a transcriptional repressor by recruiting a corepressor complex such as mSin3A/histone deacetylase 1 through association with BCL6.[36] Tissue expression of *BAZF* mRNA is restricted to heart and lung, whereas *BCL6* mRNA is expressed ubiquitously.[24,37] However, *BCL6* mRNA was barely detectable in HUVECs, whereas *BAZF* mRNA was easily detected. It has been reported that several BTB-domain–containing proteins bind specifically to CUL3, a key scaffold protein of the recently identified CUL3-based E3 ubiquitin ligase complexes, and serve as linker-adaptor proteins between CUL3 and substrates.[28-32] BAZF indeed bound CUL3 at its BTB domain, unlike CBF1 which bound BAZF at its ZnF domain. Super-resolution imaging also revealed the complete colocalization of CBF1 and CUL3 at the PML nuclear body in ECs under VEGF-A stimulation, which was completely

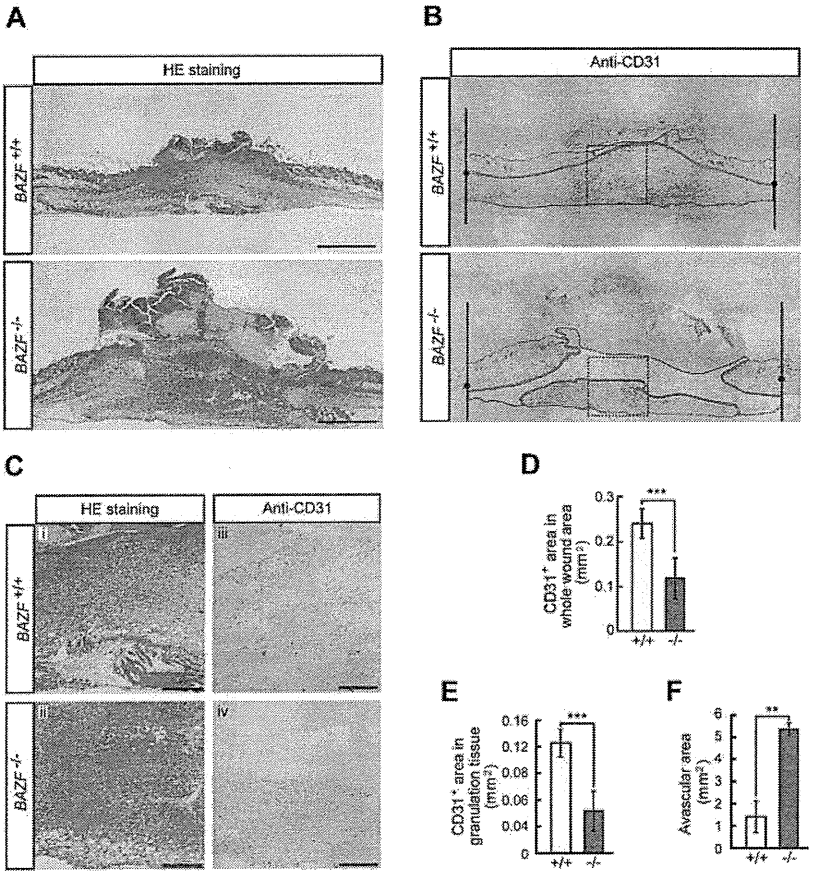

Figure 6. Impaired angiogenesis in skin wounded *BAZF*$^{-/-}$ mice. Eight-mm punch biopsies were made in the skin of the backs of 8 to 9-week-old *BAZF*$^{+/+}$ *or* *BAZF*$^{-/-}$ mice. (A) H&E staining of wound section in *BAZF*$^{+/+}$ and *BAZF*$^{-/-}$ mice at day 7. Scale bar: 2 mm. (B) Anti-CD31 staining of serial section in panel A. Green line: border of scab, magenta line: border of skin tissue, blue line: border of avascular area, red line: vascularized area in granulation tissue. (C) Magnified images of dot square regions in Figure 6B. Subpanels i and ii: H&E staining, iii and iv: anti-CD31 staining. Scale bar: 400 μm. Quantitative analysis of CD31^{+} area in whole wound area (D), CD31^{+} area in granulation tissue (E), and avascular area (F) in wound section of *BAZF*$^{+/+}$ (n = 3) and *BAZF*$^{-/-}$ (n = 3) mice was carried out using ImagePro Plus 4.5.1.

disrupted by *BAZF* knockdown. The PML nuclear body has multiple functions including proteasomal degradation,[38] suggesting that CBF1 degradation might be processing at the PML nuclear body. Furthermore, we successfully detected CBF1-CUL3 complex formation by a combination assay of immunoprecipitation and MRM analysis. These findings indicate that BAZF has a unique, BCL6-independent function in ECs. In this study, we have clearly demonstrated that BAZF functions in ECs as a linker-adaptor protein of CUL3-based E3 ubiquitin ligase complex formation targeting CBF1 as summarized in Figure 7.

In terms of phenotypic analyses in vivo, *BAZF*$^{-/-}$ mice exhibited less vessel sprouting and filopodia protrusion of tip cells as well as fewer vessel branches in the developmental retina. These phenotypic features are highly reflective of those seen in retinas of *CBF1*$^{-/-}$ mice[39] and comparable with those of mouse retinas treated with a soluble Jagged1 peptide to activate Notch,[2] implicating BAZF as a specific regulator of Notch signaling in angiogenesis. However, Notch active transgenic mice showed abnormal vasculature and the impaired dorsal aorta in embryo, which seemed to be normal in *BAZF*$^{-/-}$ mice

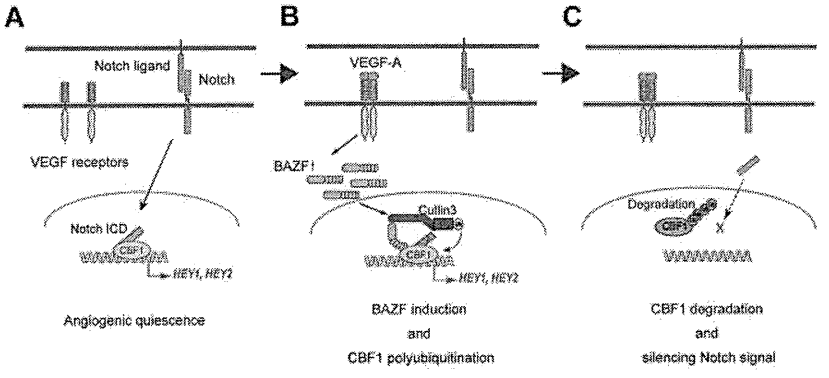

Figure 7. Model for BAZF-containing, CUL3-based E3 ligase complex as a silencer of Notch signaling for angiogenic quiescence-to-sprouting transition. (A) Degradation of CBF1 leads to silencing Notch signal and supports angiogenic sprouting. Notch signaling maintains angiogenic quiescence. Notch1 signaling is transmitted via N1ICD to CBF1. CBF1-N1ICD recruits coactivators for expression of anti-angiogenic genes. (B) BAZF-containing, CUL3-based E3 ligase complex induces CBF1 polyubiquitination. VEGF-A induces BAZF expression, and make a complex with CUL3 and CBF1 for CBF1 polyubiquitination. BAZF binding to CBF1 does not compete with N1ICD binding. However, in this step it is still unclear whether BAZF coexists with N1ICD on CBF1. (C) Degradation of polyubiquitinated CBF1. Polyubiquitinated CBF1 is released from DNA, and is degraded by proteasomes. Degradation of CBF1 leads to silencing Notch signal and supports angiogenic sprouting.

(supplemental Figure 6E-F), suggesting that BAZF might be less effective for angiogenesis in embryonic development. On the other hand, the skin-wounded *BAZF*$^{-/-}$ mice showed impaired angiogenesis, resulting in the enhanced tissue damage. Taken together, these findings suggest that BAZF functionally mediates VEGFR and Notch cross-signaling in postnatal angiogenesis involved in the tissue remodeling and repair rather than the developmental process, and that other factors to compensate BAZF might be exist in developmental stage.

Angiogenic sprouting is led by tip cells with filopodia formation and nonproliferative feature. Recent study demonstrated elegantly that dynamic position shuffling of tip and stalk cells is tightly regulated by the VEGFR-Dll4-Notch signaling circuit,[3] which consists in part of (1) Dll4 expression in ECs by VEGFR signaling,[7,14] (2) Dll4 activates Notch signaling in adjacent ECs,[2,6,10-12] (3) Nrarp-mediated negative regulation of Notch signaling,[40-43] and (4) Jagged1 expression in stalk cells, resulting in antagonizm of Dll4-mediated Notch activation in tip cells.[4] However, it is still obscure how such fine-tuned "tug-of-war" balance of VEGFR-Dll4-Notch signaling waves in tip and stalk cells would be constantly achieved.

In addition to the regulation of gene expression, the posttranslational modification of crucial factors plays a key role in regulation of cell siganlling. NICD, a key player in Notch signaling, has been shown to be acetylated, which prolonged its turnover and amplified the duration of Notch responses. NAD-dependent deacetylase SIRT1 negatively modulates Notch signaling.[44] Moreover, CBF1 is also an essential transcription cofactor of NICD, and its disruption results in spontaneous angiogenesis in retina, cornea, and internal organs such as liver and lung,[39] indicating that Notch-CBF1 signaling is an important pathway for regulation of angiogenesis, and may play an essential role in the maintenance of vascular homeostasis in adults. However, no regulation of CBF1 protein modification has been reported yet. Here we described a novel molecular mechanism underling CBF1 protein turnover regulated by VEGFR inducing BAZF-CUL3-based polyubiquitination, which might be involved in making the fine-tuned angiogenic "tug-of-war" balance between VEGFR and Notch signaling in ECs. However, it is still unclear when and how BAZF-mediated CBF1 regulation is integrated into VEGFR-Notch signaling circuit in the emergence of tip cells and filopodia formation. To understand this mechanism more precisely, the further study of the regulatory network would be essential in temporal axis.

Currently, in anti-angiogenic therapies for diabetic retinopathy, age-related macular degeneration, retinopathy of prematurity, and solid-tumor growth, Dll4-Notch signaling is becoming a prominent molecular target. Based on our studies presented here, we propose BAZF as an alternative target of Dll4-Notch signaling for future anti-angiogenesis strategies.

Acknowledgments

The authors acknowledge Dr Matsushita for insightful discussions, Mr Kawahito and Ms Ouchi (Nikon Corporation) for super-resolution imaging microscopic analysis, Mr Yokoyama (AB SCIEX) for MRM analysis, and Drs Shirakata, Iwabuki, and Yang, and Ms Tsuda for technical assistance. They are grateful to Immuno-Biologic Laboratories for providing anti-BAZF antibodies. They are also grateful to Dr Judith A. Abraham (Novartis Institutes for BioMedical Research) for helpful comments and editing the paper.

This work was supported by Grant-in-Aid for Scientific Research (20390082, 1701468, and 23112513 to S.H. and 21780312 to H.O.) from the Ministry of Education, Culture, Sports, Science and Technology, Japan, (7610010302J to S.H.) from Japan Science and Technology Agency, (6003842 to S.H.) from Strategic Young Researcher Overseas Visiting Program for Accelerating Brain Circulation, JSPS, Japan, from Incubation Project for Seeds, Ehime Industrial Promotion Foundation, and (021000 to H.O.) from Support Project for Research and Development in Ehime University.

Authorship

Contribution: H.O. performed most of the experiments assisted by H.I., H.N., S.F., and D.M.; N.T. performed mass spectrometry analysis; E.N. helped analyze gene expression by a cDNA microarray system; M.H. and T.T. provided *BAZF*$^{-/-}$ mice; Y.E. and M.N. helped design the experiments, and advised on the results; and S.H. and H.I. conceived the project, designed the experiments with H.O. and wrote the paper assisted by H.O.

Conflict-of-interest disclosure: The authors declare no competing financial interests.

Correspondence: Ehime University Graduate School of Medicine, Shitsukawa, Toon, Ehime, Japan 791-0295; e-mail: shigeki@m.ehime-u.ac.jp.

References

1. Phng LK, Gerhardt H. Angiogenesis: a team effort coordinated by notch. *Dev Cell.* 2009;16(2):196-208.
2. Hellstrom M, Phng LK, Hofmann JJ, et al. Dll4 signalling through Notch1 regulates formation of tip cells during angiogenesis. *Nature.* 2007; 445(7129):776-780.
3. Jakobsson L, Franco CA, Bentley K, et al. Endothelial cells dynamically compete for the tip cell position during angiogenic sprouting. *Nat Cell Biol.* 2010;12(10):943-953.
4. Benedito R, Roca C, Sorensen I, et al. The notch ligands Dll4 and Jagged1 have opposing effects on angiogenesis. *Cell.* 2009;137(6):1124-1135.
5. Benedito R, Trindade A, Hirashima M, et al. Loss of Notch signalling induced by Dll4 causes arterial calibre reduction by increasing endothelial cell response to angiogenic stimuli. *BMC Dev Biol.* 2008;8:117.
6. Leslie JD, Ariza-McNaughton L, Bermange AL, McAdow R, Johnson SL, Lewis J. Endothelial signalling by the Notch ligand Delta-like 4 restricts angiogenesis. *Development.* 2007;134(5):839-844.
7. Lobov IB, Renard RA, Papadopoulos N, et al. Delta-like ligand 4 (Dll4) is induced by VEGF as a negative regulator of angiogenic sprouting. *Proc Natl Acad Sci U S A.* 2007;104(9):3219-3224.
8. Noguera-Troise I, Daly C, Papadopoulos NJ, et al. Blockade of Dll4 inhibits tumour growth by promoting nonproductive angiogenesis. *Nature.* 2006;444(7122):1032-1037.
9. Ridgway J, Zhang G, Wu Y, et al. Inhibition of Dll4 signalling inhibits tumour growth by deregulating angiogenesis. *Nature.* 2006;444(7122):1083-1087.
10. Sainson RC, Aoto J, Nakatsu MN, et al. Cell-autonomous notch signaling regulates endothelial cell branching and proliferation during vascular tubulogenesis. *FASEB J.* 2005;19(8):1027-1029.
11. Siekmann AF, Lawson ND. Notch signalling limits angiogenic cell behaviour in developing zebrafish arteries. *Nature.* 2007;445(7129):781-784.
12. Suchting S, Freitas C, le Noble F, et al. The Notch ligand Delta-like 4 negatively regulates endothelial tip cell formation and vessel branching. *Proc Natl Acad Sci U S A.* 2007;104(9):3225-3230.
13. Tammela T, Zarkada G, Wallgard E, et al. Blocking VEGFR-3 suppresses angiogenic sprouting and vascular network formation. *Nature.* 2008; 454(7204):656-660.
14. Caolo V, van den Akker NM, Verbruggen S, et al. Feed-forward signaling by membrane-bound ligand receptor circuit: the case of NOTCH DELTA-like 4 ligand in endothelial cells. *J Biol Chem.* 2010;285(52):40681-40689.
15. Roukens MG, Alloul-Ramdhani M, Baan B, et al. Control of endothelial sprouting by a Tel-CtBP complex. *Nat Cell Biol.* 2010;12(10):933-942.
16. Eilken HM, Adams RH. Dynamics of endothelial cell behavior in sprouting angiogenesis. *Curr Opin Cell Biol.* 2010;22(5):617-625.

17. Higashiyama S, Nanba D, Nakayama H, Inoue H, Fukuda S. Ectodomain shedding and remnant peptide signalling of EGFRs and their ligands. *J Biochem.* 2011;150(1):15-22.
18. Zavadil J, Cermak L, Soto-Nieves N, Bottinger EP. Integration of TGF-beta/Smad and Jagged1/Notch signalling in epithelial-to-mesenchymal transition. *EMBO J.* 2004;23(5):1155-1165.
19. Takizawa T, Ochiai W, Nakashima K, Taga T. Enhanced gene activation by Notch and BMP signaling cross-talk. *Nucleic Acids Res.* 2003; 31(19):5723-5731.
20. Nakatsu MN, Sainson RC, Aoto JN, et al. Angiogenic sprouting and capillary lumen formation modeled by human umbilical vein endothelial cells (HUVEC) in fibrin gels: the role of fibroblasts and Angiopoietin-1. *Microvasc Res.* 2003;66(2): 102-112.
21. Nanba D, Mammoto A, Hashimoto K, Higashiyama S. Proteolytic release of the carboxy-terminal fragment of proHB-EGF causes nuclear export of PLZF. *J Cell Biol.* 2003;163(3): 489-502.
22. Takamori M, Hatano M, Arima M, et al. BAZF is required for activation of naive CD4 T cells by TCR triggering. *Int Immunol.* 2004;16(10):1439-1449.
23. Shirakata Y, Kimura R, Nanba D, et al. Heparin-binding EGF-like growth factor accelerates keratinocyte migration and skin wound healing. *J Cell Sci.* 2005;118(pt 11):2363-2370.
24. Okabe S, Fukuda T, Ishibashi K, et al. BAZF, a novel Bcl6 homolog, functions as a transcriptional repressor. *Mol Cell Biol.* 1998;18(7):4235-4244.
25. Williams CK, Li JL, Murga M, Harris AL, Tosato G. Up-regulation of the Notch ligand Delta-like 4 inhibits VEGF-induced endothelial cell function. *Blood.* 2006;107(3):931-939.
26. Holderfield MT, Henderson Anderson AM, Kokubo H, Chin MT, Johnson RL, Hughes CC. HESR1/CHF2 suppresses VEGFR2 transcription independent of binding to E-boxes. *Biochem Biophys Res Commun.* 2006;346(3):637-648.
27. Lubman OY, Ilagan MX, Kopan R, Barrick D. Quantitative dissection of the Notch:CSL interaction: insights into the Notch-mediated transcriptional switch. *J Mol Biol.* 2007;365(3):577-589.
28. Furukawa M, He YJ, Borchers C, Xiong Y. Targeting of protein ubiquitination by BTB-Cullin 3-Roc1 ubiquitin ligases. *Nat Cell Biol.* 2003;5(11):1001-1007.
29. Geyer R, Wee S, Anderson S, Yates J, Wolf DA. BTB/POZ domain proteins are putative substrate adaptors for cullin 3 ubiquitin ligases. *Mol Cell.* 2003;12(3):783-790.
30. Pintard L, Willis JH, Willems A, et al. The BTB protein MEL-26 is a substrate-specific adaptor of the CUL-3 ubiquitin-ligase. *Nature.* 2003; 425(6955):311-316.
31. Xu L, Wei Y, Reboul J, et al. BTB proteins are substrate-specific adaptors in an SCF-like modular ubiquitin ligase containing CUL-3. *Nature.* 2003;425(6955):316-321.
32. Pintard L, Willems A, Peter M. Cullin-based ubiquitin ligases: Cul3-BTB complexes join the family. *EMBO J.* 2004;23(8):1681-1687.
33. Broxmeyer HE, Sehra S, Cooper S, et al. Aberrant regulation of hematopoiesis by T cells in BAZF-deficient mice. *Mol Cell Biol.* 2007;27(15): 5275-5285.
34. Hartatik T, Okada S, Okabe S, Arima M, Hatano M, Tokuhisa T. Binding of BAZF and Bc16 to STAT6-binding DNA sequences. *Biochem Biophys Res Commun.* 2001;284(1):26-32.
35. Dent AL, Shaffer AL, Yu X, Allman D, Staudt LM. Control of inflammation, cytokine expression, and germinal center formation by BCL-6. *Science.* 1997;276(5312):589-592.
36. Takenaga M, Hatano M, Takamori M, et al. Bcl6-dependent transcriptional repression by BAZF. *Biochem Biophys Res Commun.* 2003;303(2): 600-608.
37. Yoshida T, Fukuda T, Hatano M, et al. The role of Bcl6 in mature cardiac myocytes. *Cardiovasc Res.* 1999;42(3):670-679.
38. Lallemand-Breitenbach V, de The H. PML nuclear bodies. *Cold Spring Harb Perspect Biol.* 2010; 2(5):a000661.
39. Dou GR, Wang YC, Hu XB, et al. RBP-J, the transcription factor downstream of Notch receptors, is essential for the maintenance of vascular homeostasis in adult mice. *FASEB J.* 2008;22(5):1606-1617.
40. Krebs LT, Deftos ML, Bevan MJ, Gridley T. The Nrarp gene encodes an ankyrin-repeat protein that is transcriptionally regulated by the notch signaling pathway. *Dev Biol.* 2001;238(1):110-119.
41. Lamar E, Deblandre G, Wettstein D, et al. Nrarp is a novel intracellular component of the Notch signaling pathway. *Genes Dev.* 2001;15(15): 1885-1899.
42. Yun TJ, Bevan MJ. Notch-regulated ankyrin-repeat protein inhibits Notch1 signaling: multiple Notch1 signaling pathways involved in T cell development. *J Immunol.* 2003;170(12):5834-5841.
43. Lahaye K, Kricha S, Bellefroid EJ. XNAP, a conserved ankyrin repeat-containing protein with a role in the Notch pathway during Xenopus primary neurogenesis. *Mech Dev.* 2002;110(1-2): 113-124.
44. Guarani V, Deflorian G, Franco CA, et al. Acetylation-dependent regulation of endothelial Notch signalling by the SIRT1 deacetylase. *Nature.* 2011;473(7346):234-238.

Journal of Histochemistry & Cytochemistry 59(7) 673–689

DOI: 10.1369/0022155411408906
http://jhc.sagepub.com
SAGE

Specific In Situ Visualization of Plasma Cells Producing Antibodies against *Porphyromonas gingivalis* in Gingival Radicular Cyst: Application of the Enzyme-Labeled Antigen Method

Shinya Tsuge, Yasuyoshi Mizutani, Kazuhiro Matsuoka, Tatsuya Sawasaki, Yaeta Endo, Koji Naruishi, Hiroshi Maeda, Shogo Takashiba, Kazuya Shiogama, Ken-ichi Inada, and Yutaka Tsutsumi

Departments of Pathology (STsuge,YM,KS,KI,YT) and Oral and Maxillofacial Surgery (STsuge), Fujita Health University School of Medicine, Toyoake, Aichi, Japan; Cell-Free Science and Technology Research Center, Ehime University, Matsuyama, Japan (KM,TS,YE); Proteo-Medicine Research Center, Ehime University, Toon, Japan (TS,YE); and Department of Pathophysiology–Periodontal Science, Okayama University Graduate School of Medicine, Dentistry and Pharmaceutical Sciences, Okayama, Japan (KN,HM,STakashiba)

Summary

The enzyme-labeled antigen method was applied to visualize plasma cells producing antibodies to *Porphyromonas gingivalis*, flora of the human oral cavity. Antibodies to *P. gingivalis* have reportedly been detected in sera of patients with periodontitis. Biotinylated bacterial antigens, Ag53, and four gingipain domains (Arg-pro, Arg-hgp, Lys-pro, and Lys-hgp) were prepared by the cell-free protein synthesis system using the wheat germ extract. In paraformaldehyde-fixed frozen sections of rat lymph nodes experimentally immunized with Ag53-positive and Ag53-negative *P. gingivalis*, plasma cells were labeled with biotinylated Arg-hgp and Lys-hgp. Antibodies to Ag53 were detected only in the nodes immunized with Ag53-positive bacteria. In two of eight lesions of gingival radicular cyst with inflammatory infiltration, CD138-positive plasma cells in frozen sections were signalized for Arg-hgp and Lys-hgp. An absorption study using unlabeled antigens confirmed the specificity of staining. The AlphaScreen method identified the same-type antibodies in tissue extracts but not in sera. Antibodies to Ag53, Arg-pro, and Lys-pro were undetectable. In two cases, serum antibodies to Arg-hgp and Lys-hgp were AlphaScreen positive, whereas plasma cells were scarcely observed within the lesions. These findings indicate the validity of the enzyme-labeled antigen method. This is the very first application of this novel histochemical technique to human clinical samples. (J Histochem Cytochem 59:673–689, 2011)

Keywords

enzyme-labeled antigen method, AlphaScreen method, cell-free protein synthesis, radicular cyst, *Porphyromonas gingivalis*, Ag53, gingipains

A variety of infectious, autoimmune, and neoplastic lesions contain numerous antibody-producing plasma cells as part of inflammatory cells. In most cases, target antigens of the antibodies produced by these plasma cells in the lesion remain unknown. The antibodies produced within the lesion should directly be related to pathogenesis.

The enzyme-labeled antigen method is a reversed form of the enzyme-labeled antibody method or immunoperoxidase technique. This histochemical technique was first proposed as early as 1968, in an experimental model to detect anti–horseradish peroxidase (HRP) antibody-producing cells in the lymph nodes of rats immunized with HRP (Leduce et al. 1968; Straus 1968). However, no further application has been reported since we revived this technique in 2009 to visualize the

Received for publication January 15, 2011; accepted March 29, 2011

Corresponding Author:
Yutaka Tsutsumi, MD, Department of Pathology, Fujita Health University School of Medicine, Toyoake, Aichi 470-1192, Japan.
E-mail: tsutsumi@fujita-hu.ac.jp

site of specific antibody production in the lymph nodes and spleen of rats immunized with HRP, keyhole limpet hemocyanin (KLH), and ovalbumin (Mizutani et al. 2009). Biotinylated KLH and ovalbumin were prepared as probes for this technique. When the labeled antigen is available, the enzyme-labeled antigen method can thus visualize the site of antibody production in sections of human clinical samples.

In the present study, we analyzed the site of antibody production against *Porphyromonas gingivalis* (*Bacteroides gingivalis*) in human surgical specimens of gingival radicular cyst. *P. gingivalis* is a black-pigmented, non-motile, obligatory anaerobic gram-negative bacillus normally residing in the human oral cavity and abnormally colonizing in lesions of pyorrheal gingivitis/periodontitis (Cutler et al. 1995; Lamont and Jenkinson 1998; Holt et al. 1999; Slots and Ting 1999). Biofilm formation was noted when colonizing in the gingival lesion (Lamont and Jenkinson 1998). Antibodies to *P. gingivalis* have been detected in the serum of patients with periodontitis (Kurihara et al. 1991; Schenkein 2006). Radicular cyst, also called an apical cyst, is associated with dental caries and often shows marked inflammatory reaction with dense plasma cell infiltration (Dahlen 2002). Microbiological analysis of radicular cyst indicated some 50 species of bacterial colonization, mainly anaerobes such as *Porphyromonas* (or *Bacteroides*), *Fusobacterium*, *Tannerella*, *Prevotella*, *Peptostreptococcus*, *Actinomyces*, and so on (Jung et al. 2000; Dahlen 2002; Wayman et al. 2002; Sunde et al. 2003; Noguchi et al. 2005).

The enzyme-labeled antigen method was herein applied to demonstrating plasma cells producing specific antibodies to *P. gingivalis*–related antigens in prefixed frozen sections of radicular cyst. We chose the following five proteins as target antigens, including Ag53, a 53-kDa membrane-associated protein (Kurihara et al. 1991; Oyaizu et al. 2001), and *P. gingivalis*–associated cysteine proteases, Arg-gingipain and Lys-gingipain (Chen et al. 2001; O'Brien-Simpson et al. 2001; Grenier and Tanabe 2010). Rat lymph nodes experimentally immunized with Ag53-positive and Ag53-negative *P. gingivalis* were also successfully evaluated.

For effectively preparing biotin-labeled antigens, we used the cell-free protein synthesis system using the wheat germ extract, which has been established by the Cell-Free Science and Technology Research Center, Ehime University (Sawasaki, Hasegawa, et al. 2002). The specific antibodies in the serum were easily identified with the AlphaScreen method (Matsuoka et al. 2010).

Application of the enzyme-labeled antigen method may help the pathogenesis be solved. Plasma cells infiltrating in the lesion of autoimmune disease should produce autoantibodies, those in the infectious lesion should produce antibodies against pathogens, and those in the neoplastic lesion may produce antibodies against tumor cells. Once the labeled antigen is available, our methodology may have powerful potential in morphological and histochemical research and also in clinicopathological applications.

Material and Methods

Bacterial Strains and Growth Condition

Two strains of *P. gingivalis* ATCC33277 and FDC381 and *Streptococcus mutans* 854S were obtained from American Type Culture Collection (Manassas, VA). *P. gingivalis* ATCC33277 lacks Ag53 expression (Naito et al. 2008), and FDC381 expresses Ag53 (Oyaizu et al. 2001). The bacteria were maintained under anaerobic conditions in the Department of Pathophysiology–Periodontal Science, Okayama University Graduate School of Medicine, Dentistry and Pharmaceutical Sciences, Okayama, Japan. Briefly, *P. gingivalis* was grown in GAM broth (Nissui Seiyaku, Tokyo, Japan) supplemented with 0.0005% hemin and 0.0001% vitamin K3 at 37C for 24 to 48 hr in an anaerobic box (model ANX-1; Hirasawa Works, Tokyo, Japan) containing 80% N_2, 10% H_2, and 10% CO_2, as previously described (Kato et al. 2008). *S. mutans* was grown in Tripticate Soy Broth (BD Biosciences, San Jose, CA) supplemented with 0.5% yeast extract (BD Biosciences), as previously described (Yoshida and Kuramitsu 2002). DNA was purified from *P. gingivalis* FDC381 and *S. mutans* 854S.

Experimental Animals

Male Sprague Dawley rats aged 5 weeks and weighing 150 g (Chubu Kagaku, Nagoya, Japan) were kept in the animal laboratory of Fujita Health University, Toyoake, Japan. The animal experiments were conducted in accordance with the Guidelines for the Management of Laboratory Animals at Fujita Health University (acknowledgment no. M2104, April 2008).

Immunization and Tissue Sampling

The animals were immunized with two strains of *P. gingivalis*, Ag53 positive and Ag53 negative. The boiled bacteria emulsified in Freund's complete (first challenge) or incomplete (second and third challenges) adjuvant were injected three times in 5 weeks into footpads of the rats (n=3 in the respective group), and the axillary and popliteal lymph nodes, as well as the serum, were sampled 14 days after the third immunization. Rats (n=2) immunized only with Freund's adjuvant served as negative controls.

Under the diethyl ether anesthesia, part of the axillary and popliteal lymph nodes was sampled and fixed in buffered 4% paraformaldehyde, pH 7.2, at 4C for 4 hr to prepare frozen sections on a cryostat. The remaining part of the lymph nodes was homogenized in 10 mM phosphate-buffered saline (PBS), pH 7.2, to prepare tissue extracts. Blood was sampled from renal veins of the rats. The sera were separated by centrifugation for 10 min at 3,000 rpm and stored at –80C until use.

Western Blotting

Western blotting was performed, as previously described (Kato et al. 2008). *P. gingivalis* or *S. mutans* was totally lysed by adding 100 μL of 6× sodium dodecyl sulfate (SDS) sample buffer to 500 μL of the reaction mixture, and then boiling the samples for 5 min followed. The final composition of SDS sample buffer after mixing was 2% SDS, 58.3 mM Tris-HCl (pH 6.8), 6% glycerol, 5% 2-mercaptoethanol, 0.002% bromophenol blue, and protease inhibitor mix (Complete TM; Roche Applied Science, Indianapolis, IN). Aliquots of these samples (10 μg/lane) were separated by SDS–polyacrylamide gel electrophoresis on 12% polyacrylamide slab gels. The separated proteins were immediately transferred electrophoretically to polyvinylidene difluoride (PVDF) membranes (Millipore, Bedford, MA) using TB buffer (25 mM Tris, 192 mM glycine, and 20% methanol, pH 8.4). Proteins were transferred at 100 V for 1 hr at 4C. Membranes were blocked for 1 hr at room temperature with 5% skim milk in TBST (20 mM Tris-HCl, pH 7.6, containing 150 mM NaCl and 0.05% Tween-20). The blocking buffer was removed, and the membranes were incubated with the appropriate primary antiserum (the serum of *P. gingivalis*–immunized rat or control rat; 1:100,000 dilution) at 4C overnight in the blocking buffer. The membranes were subsequently washed three times (10 min/wash) with TBST and then incubated with the secondary antibody (goat anti-rat IgG-HRP conjugate, GE Healthcare, Piscataway, NJ; 1:100,000 dilution) in the blocking buffer for 1 hr at room temperature. After rinsing three times in TBST, the HRP activity was visualized by incubating the membranes for 5 min at room temperature in Super Signal West Pico Chemiluminescent Substrate detection system (Pierce, Rockford, IL) followed by autoradiography. At the end of these experiments, the membranes were stained with Coomassie brilliant blue (Bio-Rad, Hercules, CA) to confirm that equal amounts of protein were loaded in each lane of the gel.

Patients and Surgical Specimens

A total of 10 patients (M:F = 6:4) suffering from dental caries–associated radicular cyst were recruited. The age of the patients ranged from 28 to 60 years (mean, 46). Six occurred in the upper jaw and four in the mandible. Incisor teeth were affected in five cases, followed by molar (n=4) and premolar (n=1). The size varied from 0.8 to 3.4 cm (mean, 2.0) in diameter. The association of periodontitis was evaluated on X-ray film according to the degree of absorption of the alveolar bone. Periodontitis was graded as none (n=4), mild (n=2), moderate (n=4), and severe (n=0).

The surgical specimens of radicular cyst were divided into three pieces. Half was fixed in 10% formalin for histopathological diagnosis. The remaining tissue portions were used for preparing both fixed frozen sections and tissue extracts in the same way as for the rat experiment. Of 10 surgical specimens of radicular cyst, 8 showed dense infiltration of plasma cells within the lesions. Tissue extraction was performed in 6. The serum was sampled from the respective cases.

Written informed consent was obtained from each patient, and the analysis using human specimens was authorized by the Committee of Ethics for Clinical and Epidemiological Study, Fujita Health University School of Medicine (acknowledgment no. 07-102, October 2007).

Target Bacterial Proteins (Antigens)

In the present study, a total of five proteins derived from *P. gingivalis* were analyzed: These included Ag53 and four gingipain components such as the proteinase domain of Arg-gingipain (Arg-pro), the hemagglutinin/adhesin domain of Arg-gingipain (Arg-hgp), the proteinase domain of Lys-gingipain (Lys-pro), and the hemagglutinin/adhesin domain of Lys-gingipain (Lys-hgp). For the negative control purpose, SpaP, a representative pathogenic protein derived from *S. mutans* and dihydrofolate reductase (DHFR) of *Escherichia coli* origin were evaluated. The molecular weight of the respective proteins is as follows: Ag53 = 53 kDa, Arg-pro = 44 kDa, Arg-hgp = 103 kDa, Lys-pro = 51 kDa, Lys-hgp = 103 kDa, SpaP = 185 kDa, and DHFR = 24 kDa.

Plasmid Construction for the Cell-Free Protein Synthesis

Six bacterial genes encoding Ag53, Arg-pro, Arg-hgp, Lys-pro, Lys-hgp, and SpaP were amplified from genomic DNA of *P. gingivalis* FDC381 or *S. mutans* 854S by polymerase chain reaction (PCR) with PrimeStar HS DNA polymerase (Takara Bio, Otsu, Japan) or Ex Taq polymerase (Takara Bio), using the primers as indicated in Table 1. The sense primers contained the restriction enzyme recognition sequence (*Sal*I or *Xho*I) and biotin ligase recognition sequence, whereas the restriction enzyme recognition site (*Not*I) was included in the antisense primers. The PCR products were digested with *Sal*I and *Not*I or *Xho*I and *Not*I and then cloned into the corresponding sites of the pEU-E01-His-MCS vector (CellFree Sciences, Matsuyama, Japan). Nucleotide sequences of the DNA inserts in all plasmid constructs were subsequently confirmed by using the ABI PRISM 310 Genetic Analyzer using the BigDye terminator v1.1 Cycle sequence kit (Applied Biosystems, Foster City, CA). Plasmid DNA for transcription reactions was purified using Plasmid Midi Kit (QIAGEN, Stanford, CA).

The DHFR gene of *E. coli* was also PCR amplified (Sawasaki, Ogasawara, et al. 2002) with LA Taq polymerase (Takara Bio) using the primers, as indicated in Table 1. The PCR product was digested with *Xho*I and *Spe*I and then cloned into the corresponding sites of the

Table 1. The sequences of the primer pairs used for PCR amplification of *P. gingivalis*-related proteins, SpaP and DHFR

Target Gene	Sense/ Antisense	Restriction Site	Sequence
Ag53	Sense	*Sal*I	GAGA**GTCGAC**ATGGGCCTGAACGACATCTTCGAGGCCCAGAA GATCGAGTGGCACGAAATGAAGTTAAACAAAATGTT
	Antisense	*Not*I	GAGA**GCGGCCGC**TTAGAATTCGATATCATAGTTATG
Arg-pro	Sense	*Xho*I	GAGA**CTCGAG**ATGGGCCTGAACGACATCTTCGAGGCCCAGAAGATCGAGTGG CACGAATACACACCGGTAGAGGAAAAAC
	Antisense	*Not*I	GAGA**GCGGCCGC**TTAGCGAAGAAGTTCGGGGGCATCGC
Arg-hgp	Sense	*Xho*I	GAGA**CTCGAG**ATGGGCCTGAACGACATCTTCGAGGCCCAGAAGATCGAGT GGCACGAAAGCGGTCAGGCCGAGATTGTTC
	Antisense	*Not*I	GAGA**GCGGCCGC**TTACTTTACAGCGAGTTTCTC
Lys-pro	Sense	*Xho*I	GAGA**CTCGAG**ATGGGCCTGAACGACATCTTCGAGGCCCAGAAGATCGAGT GGCACGAAGATGTTTATACAGATCATGGCG
	Antisense	*Not*I	GAGA**GCGGCCGC**TTAACGTACATCGTTTGCAGGTTC
Lys-hgp	Sense	*Xho*I	GAGA**CTCGAG**ATGGGCCTGAACGACATCTTCGAGGCCCAGAAGATCGAGT GGCACGAAGCCAACGAAGCCAAGGTTGTGC
	Antisense	*Not*I	GAGA**GCGGCCGC**TTACTTGATAGCGAGTTTCTC
SpaP	Sense	*Xho*I	GAGA**CTCGAG**ATGGGCCTGAACGACATCTTCGAGGCCCAGAAGATCGAGT GGCACGAAATGAAAGTCAAAAAAACTTACGG
	Antisense	*Not*I	GAGA**GCGGCCGC**TCAATCTTTCTTAGCCTTTAAG
DHFR	Sense	*Xho*I	GAGA**CTCGAG**GGCCTGAACGACATCTTCGAGGCCCAGAAGATCGAGTGG CACGAACTCCACCCACCACCACCAATGATCAGTCTGATTGCGGC
	Antisense	*Spe*I	GAGA**ACTAGT**TTACCGCCGCTCCAGAATCT

Bold: restriction enzyme recognition sequence. Underline: biotin ligase recognition sequence.

pEU-E01-His-MCS vector. Nucleotide sequence analysis and plasmid DNA purification were carried out as mentioned above.

Cell-Free Protein Synthesis System

The cell-free protein synthesis system has been established in the Cell-Free Science and Technology Research Center, Ehime University (Sawasaki, Hasegawa, et al. 2002; Sawasaki, Ogasawara, et al. 2002). Briefly, the wheat germ extract (ENDEXT kits; CellFree Sciences) effectively synthesized proteins encoded by genomic bacterial DNA in 96-well plastic plates. The plasmid vectors, incorporated with target DNA and the biotin ligase recognition sequence, were harvested from *E. coli* and used as templates for the protein synthesis. Transcription by SP6 RNA polymerase to yield messenger RNA (mRNA) and translation to yield protein products using the wheat germ extract followed. Finally, biotin labeling was performed through biotin ligase activity to obtain a target protein that a single biotin was labeled on the *N*-terminal site. The *N*-terminally biotin-labeled target proteins lacking sugar residues functioned as probes for the enzyme-labeled antigen method. The translation mixtures were directly used without purification or concentration.

For biotin labeling of proteins, the previously described bilayer diffusion system was employed (Sawasaki, Hasegawa, et al. 2002; Sawasaki et al. 2008; Matsuoka et al. 2010). Briefly, 2 μg of biotin protein ligase (BirA, GenBank accession no. NP0312927) produced by the wheat cell-free system was added to the translation layer, and 5 μM D-biotin (Nacalai Tesque, Kyoto, Japan) were supplemented to both the translation and substrate layers.

Purification of Bacterial Proteins

Purification of biotinylated proteins (Sawasaki et al. 2008; Matsuoka et al. 2010) was performed for Ag53, Arg-pro, Arg-hgp, Lys-pro, Lys-hgp, and DHFR to compare the efficiency as the primary reagent and to know the appropriate concentration as the probe for the enzyme-labeled antigen method.

For purification, a polyhistidine tag was added to the *N*-terminal of the biotinylated proteins on a specialized vector (pEU-E01-His-bls-ORF subcloned from pEU-E01-His-MCS). Ni^{2+}-affinity chromatography using Ni-NTA sepharose (GE Healthcare) was employed for one-step purification of the tagged proteins. The elution buffer contained 20 mM Na-phosphate (pH 7.5), 0.3 M NaCl, and 500 mM imidazole (Nacalai Tesque). The purified biotinylated

proteins (concentrations around 200 μg/mL) were electrophoresed on polyacrylamide gel under SDS, and Coomassie brilliant blue staining for proteins was done. The separated proteins were also transferred to a Hybond-LFP PVDF membrane (GE Healthcare). After blocking with 5% skim milk in PBS at 4C overnight, the membranes were soaked in PBS containing 2 μg/mL streptavidin Alexa Fluor 488 conjugate (STA–Alexa 488; Invitrogen, Carlsbad, CA) and were rinsed three times with PBS containing 0.05% Tween-20. The biotinylated proteins on membranes were detected by the Typhoon 9400 imaging system (GE Healthcare), according to the manufacturer's protocol.

The cell-free protein synthesis and polyhistidine-tagged protein purification using imidazole buffer for elution were carried out using an automatic robot, Protemist DTII (CellFree Sciences), basically according to the manufacturer's instructions. The processes of in vitro transcription (for 6 hr), synthesis of biotinylated proteins (for 20 hr), and purification (for 4–6 hr) were automated with this machine.

The AlphaScreen Method

The AlphaScreen assay (Xu et al. 2009; Matsuoka et al. 2010) was performed at the Cell-Free Science and Technology Research Center, Ehime University, according to the manufacturer's protocol (PerkinElmer Life and Analytical Sciences, Boston, MA). Reactions were carried out in 25 μL of reaction volume in 384-well Optiwell microtiter plates (PerkinElmer Life and Analytical Sciences). For the antigen-antibody reaction, the translation mixture containing the biotinylated protein was mixed with the 1:600 diluted sera or 1:300 diluted tissue extracts of patients and rats in 15 μL of reaction buffer (100 mM Tris-HCl, pH 8.0, containing 0.01% Tween-20 and 0.1% bovine serum albumin) and incubated at 26C for 30 min. Subsequently, 10 μL of streptavidin-coated donor beads and protein G-conjugated acceptor beads (PerkinElmer Life and Analytical Sciences) was added to a final concentration at 12 μg/mL per well and incubated at 26C for 1 hr in a dark box. Fluorescence emission was measured with the EnVision plate reader (PerkinElmer Life and Analytical Sciences), and the resultant data were analyzed using the AlphaScreen detection program. All repetitive mechanical procedures were performed by a Biomek FX robotic workstation (Beckman Coulter, Fullerton, CA).

Only when the antibodies were reactive with the *N*-terminally biotinylated antigens, fluorescent signals at 520 to 620 nm emitted. The wells with antigen-antibody reaction were thus easily recognized. The data were expressed as the signal intensity ratio when compared with the DHFR control (basal level) (Sawasaki, Hasegawa, et al. 2002; Sawasaki, Ogasawara, et al. 2002; Matsuoka et al. 2010). In the present study, a ratio no less than 2.0 was regarded as positive.

Enzyme-Labeled Antigen Method

Paraformaldehyde-fixed frozen sections with or without proteinase K pretreatment were incubated for 1 hr at room temperature with unpurified crude solutions (translation mixtures) containing biotinylated proteins, which were synthesized in the cell-free protein synthesis system in the well. HRP-labeled streptavidin was incubated as the secondary reagent for 1 hr at room temperature. After rinsing with PBS, the site of antigen-antibody reaction was visualized in 50 mM Tris-HCl buffer, pH 7.6, containing 20 mg/dL diaminobenzidine hydrochloride and 0.006% hydrogen peroxide. The nuclei were lightly counterstained with Mayer's hematoxylin.

The effect of proteinase K pretreatment was evaluated by comparing with untreated sections. In the present study, we employed the digestion with 4 μg/mL proteinase K in 50 mM Tris-buffered saline, pH 7.6, for 15 min at room temperature, as reported previously (Mizutani et al. 2009).

To know the suitable concentration of the antigen solution for this technique, purified biotinylated proteins of Ag53, Arg-hgp, and Lys-hgp were incubated at the final concentrations of 1, 10, 50, and 100 μg protein/mL. For the human study, purified antigens were used on most occasions, except for SpaP.

Double Immunofluorescence Study

Double immunofluorescence staining was performed to show that cells labeled with biotinylated antigens express CD138 (syndecan-1) on the plasma membrane. CD138 is a known plasma cell marker, although epithelial cells are also labeled (Sebestyén et al. 1999). Sections were incubated with 1:100 diluted mouse anti-human CD138 monoclonal antibody (clone MI15; Dako, Glostrup, Denmark) and then with Alexa Fluor 568 (red)–labeled goat anti-mouse IgG antibody (Invitrogen, Eugene, OR). Subsequently, the sections were incubated with biotinylated antigens and next with Alexa Fluor 488 (green)–labeled streptavidin (Invitrogen). Proteinase K treatment was omitted to retain CD138 immunoreactivity. In every step, the reagents were incubated for 1 hr at room temperature. Finally, the sections were mounted in hydrophilic mounting medium (Prolong Gold Antifade Reagent with DAPI, Invitrogen). The nuclei were stained blue with 4′,6-diamidino-2′-phenylindole (DAPI). The immunofluorescence was observed under a microscope (AXIO Imager A1; Carl Zeiss, Oberkochen, Germany).

Absorption Experiment

To confirm the specificity of the enzyme-labeled antigen method, we performed the absorption experiment. We

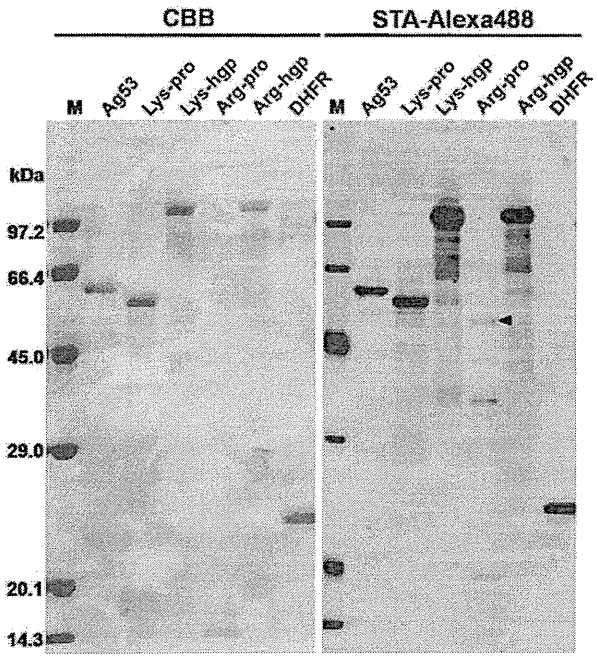

Figure 1. Electrophoretic analysis of purified biotinylated proteins used in the present study. Protein bands showing appropriate molecular weights are visualized with both Coomassie brilliant blue (CBB) staining (left panel) and Western blot analysis using streptavidin–Alexa 488 (STA-Alexa488) (right panel). The estimated molecular weight of the proteins is Ag53 = 53 kDa, Lys-pro = 51 kDa, Lys-hgp = 103 kDa, Arg-pro = 44 kDa, Arg-hgp = 103 kDa, and DHFR = 24 kDa. The band of Arg-pro is relatively weak (arrowhead in the right panel). M, molecular weight markers.

prepared five kinds of crude unlabeled antigen solutions (Ag53, Arg-hgp, Lys-hgp, Arg-pro, and Lys-pro) by the cell-free wheat germ system. The crude biotinylated antigen solutions (Ag53, Arg-hgp, and Lys-hgp) were diluted with the unlabeled antigen solutions or PBS at 1:5, and plasma cells producing antibodies to Ag53, Arg-hgp, or Lys-hgp in rat lymph nodes and human radicular cyst lesions (cases 3 and 6) were visualized. Expectedly, an excess amount of the corresponding antigens abolished the specific staining, but indifferent antigens did not.

Results

Synthesis and Purification of Bacterial Proteins

Five *P. gingivalis* proteins, including Ag53, Arg-pro, Arg-hgp, Lys-pro, and Lys-hgp, as well as SpaP and DHFR as controls, were synthesized and biotinylated with the cell-free, wheat germ extract–mediated protein synthesis system. Crude solutions (translation mixtures) in the wells were used for screening for the enzyme-labeled antigen method and the absorption experiment. To obtain purified biotinylated proteins (except for SpaP), polyhistidine-tagged proteins were harvested by reacting in multiple wells.

Figure 1 demonstrates results of the electrophoretic analysis of the purified biotinylated proteins. Protein bands showing appropriate molecular weights were visualized with both Coomassie brilliant blue staining and Western blot analysis using streptavidin–Alexa 488.

Rat Experiment

Western Blotting

Western blot analysis was performed to analyze reactivity of sera of the immunized rats against bacterial lysates (Fig. 2). Multiple bands were seen on the blot membrane when *P. gingivalis* ATCC33277-injected rat sera (n=3) were reacted to *P. gingivalis* lysates, whereas no bands were observed against *S. mutans* 854S lysates. The sera of the control rats injected adjuvant alone (n=2) were also unreactive.

AlphaScreen Method

When the signal intensity ratio relative to the DHFR control was no less than 2.0, the signals in the AlphaScreen method were regarded as positive. The extracts of axillary and popliteal lymph nodes of rats immunized with Ag53-positive and Ag53-negative *P. gingivalis*, as well as the extracts from the control rats, were evaluated. The sera of rats immunized with Ag53-positive bacteria and of control rats were also checked by the AlphaScreen method. The sera of rats immunized with Ag53-negative bacteria, used for the Western blot analysis, were not examined.

As shown in Table 2, in two of three of rats immunized with Ag53-negative *P. gingivalis*, the antibodies to Arg-hgp and Lys-hgp were detected in the lymph node extract with the AlphaScreen method, whereas antibodies to Ag53, Arg-pro, Lys-pro, and SpaP were undetectable. In all three rats immunized with Ag53-positive bacteria, antibodies to Ag53 were raised in the lymph node extract and serum, whereas antibody titers against gingipain-related proteins were below the cutoff level. No antibody elevation was noted in the lymph node extracts and sera of the control rats (n=2).

Unpurified Protein Solutions as Probes for the Enzyme-Labeled Antigen Method and the Effect of Proteinase K Pretreatment

At first, we checked the crude biotinylated protein solutions (the supernatant of the cell-free translation mixture in each well) as probes for the enzyme-labeled antigen method. In fixed frozen sections of the lymph nodes of rats immunized with Ag53-positive *P. gingivalis*, the cytoplasm of plasma cells was positively labeled with biotinylated Ag53, Arg-hgp, and Lys-hgp. Then, the effectiveness of proteinase K pretreatment was evaluated. Proteinase K (4 μg/mL) pretreatment for 15 min at room temperature increased detectability of the specific antibody in plasma cells in fixed frozen sections (Fig. 3). Inhibition of endogenous peroxidase and endogenous biotin activities was

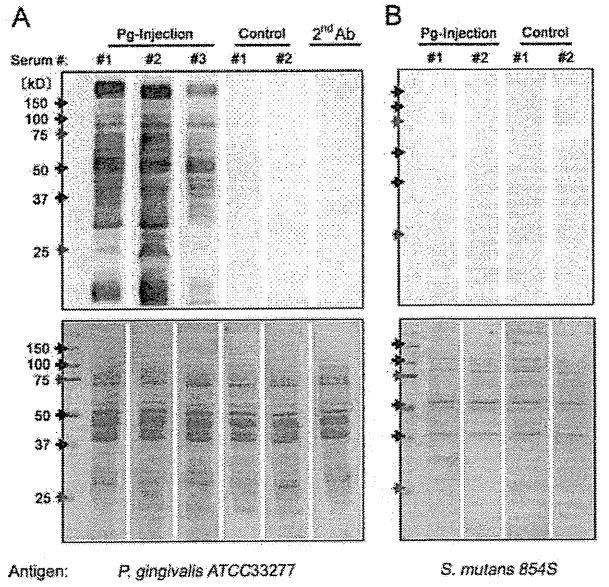

Figure 2. Western blot analysis of bacterial lysates with immunized rat sera. Upper panels: autoradiographic demonstration of antibodies to *Porphyromonas gingivalis* in rat sera. Lower panels: Coomassie brilliant blue staining. (a) The sera of Ag53-negative *P. gingivalis* ATCC33277-injected rats (n=3) showed multiple bands reactive to the whole-cell lysates of *P. gingivalis*, but the sera of control rats injected adjuvant alone (n=2) did not. (b) The sera of *P. gingivalis*–injected and control rats did not react to the whole-cell lysates of *Streptococcus mutans*.

confirmed by the negativity in proteinase K–pretreated negative control sections incubated with buffer alone.

Evaluation of Appropriate Concentration of Biotinylated Antigen Solution

In rat lymph nodes with positive signals, the appropriate concentration of the biotinylated antigen solution was evaluated. For this purpose, purified biotinylated proteins of Ag53, Arg-hgp, and Lys-hgp (original protein concentration around 200 μg/mL) were used, and the antigen solutions adjusted with concentrations of 1, 10, 50, and 100 μg/mL were applied to fixed frozen sections. The concentration at 100 μg/mL gave the best result for Ag53, whereas 50 μg/mL was regarded suitable for detecting antibodies against Arg-hgp and Lys-hgp in frozen sections (Fig. 4).

We decided to use purified Arg-pro and Lys-pro with a concentration at 50 μg/mL for further study because the original concentration of the purified proteins was around 70 μg/mL.

Application of the Enzyme-Labeled Antigen Method to Rat Lymph Nodes

By the enzyme-labeled antigen method, antibodies specific to Arg-hgp and Lys-hgp were consistently demonstrated in plasma cells in the axillary and popliteal lymph nodes of all rats (n=6) immunized with Ag53-positive and Ag53-negative *P. gingivalis*. A good number of positively labeled

Table 2. Summary of the AlphaScreen Method and the Enzyme-Labeled Antigen Method in the Rat Experiment

	Serum					Tissue Extract														
Ag	Control		Ag53(+)Pg			Control				Ag53(–)Pg						Ag53(+)Pg				
Animal	1	2	1	2	3	1		2		1		2		3		1		2		3	
Site						Ax	Po	Ax	Po	Ax	Po	Ax	Po	Ax	Po	Ax	Po	Ax	Po	Ax	Po
AlphaScreen method																					
Ag53	1.1	1.1	**7.7**	**9.5**	**20.5**	1.3	1.5	1.2	1.5	1.4	1.1	1.2	1.1	1.4	1.0	1.9	**2.2**	**3.0**	**2.9**	**4.4**	NE
Arg-pro	1.0	0.9	0.9	1.3	1.1	1.0	1.2	1.0	1.0	1.1	0.9	0.9	0.9	1.2	1.0	0.9	1.0	0.9	1.0	1.1	NE
Arg-hgp	0.9	1.0	**3.3**	**4.2**	**4.4**	1.0	1.1	1.0	1.0	1.9	1.3	1.5	**2.9**	**3.0**	**2.5**	1.3	1.4	1.5	1.4	1.5	NE
Lys-pro	0.9	1.0	1.1	1.4	1.2	1.0	1.3	1.1	1.1	1.2	1.0	1.0	1.0	1.1	1.0	0.9	1.1	1.0	0.9	1.1	NE
Lys-hgp	1.0	1.0	**3.5**	**4.0**	**5.1**	1.1	1.4	1.1	1.3	1.6	1.2	1.3	**2.1**	**2.8**	**2.2**	1.2	1.3	1.3	1.2	1.6	NE
SpaP	0.9	0.9	1.0	1.2	0.9	1.0	1.0	0.9	1.1	1.1	0.9	0.8	1.0	1.2	0.9	1.0	0.9	1.1	0.9	1.1	NE
Enzyme-labeled antigen method																					
Ag53						–	–	–	–	–	–	–	–	–	–	+	+	+	+	+	+
Arg-pro						–	–	–	–	–	–	–	+	–	–	–	–	–	–	–	–
Arg-hgp						–	–	–	–	+	+	+	+	+	+	+	+	–	+	+	+
Lys-pro						–	–	–	–	–	–	–	–	–	–	–	–	–	–	–	–
Lys-hgp						–	–	–	–	+	+	+	+	+	+	+	+	+	+	+	+
SpaP						–	–	–	–	–	–	–	–	–	–	–	–	–	–	–	–

Ag53(+)Pg, Ag53-positive *Porphyromonas gingivalis* immunized rats; Ag53(–)Pg, Ag53-negative *P. gingivalis* immunized rats; Ax, axillary lymph node; Po, popliteal lymph node; NE, not examined. No serum was evaluated in Ag53(–)Pg. AlphaScreen method: Data no less than 2.0 are regarded as positive, represented with bold figures. + indicates positive reaction with the enzyme-labeled antigen method.

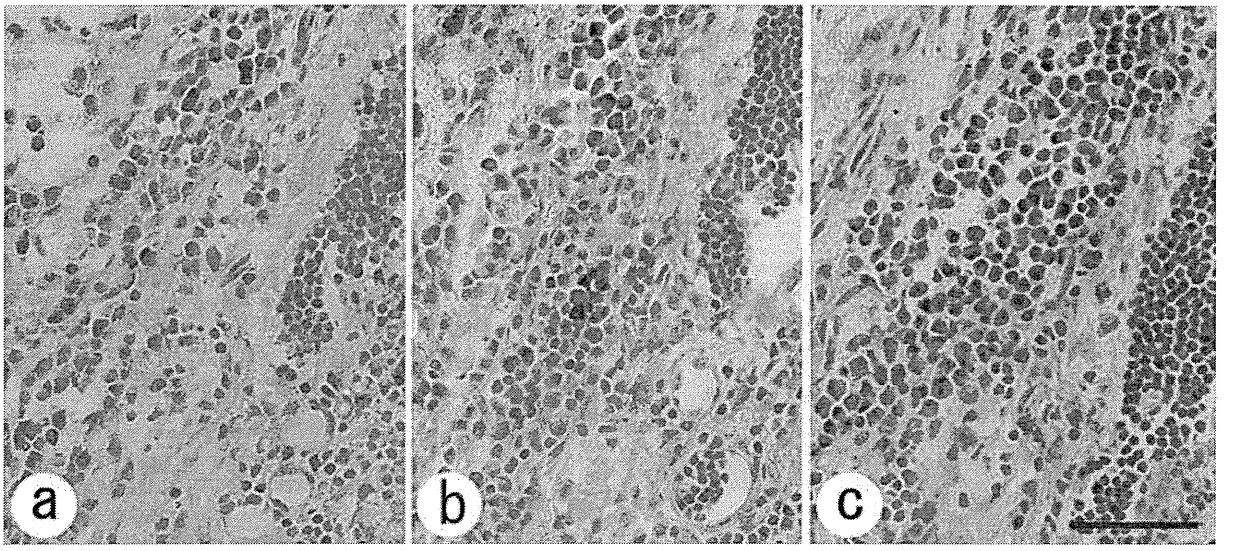

Figure 3. The effect of proteinase K pretreatment (4 μg/mL, for 15 min at room temperature) to retrieve the reactivity in the enzyme-labeled antigen method. Unpurified translation mixtures recruited from the cell-free wheat germ extract system were used as probes. Plasma cells in rat axillary lymph node immunized with Ag53-positive *Porphyromonas gingivalis* exhibit production of anti-Ag53 antibodies. When compared with the untreated frozen section (a), the reactivity is stronger in the proteinase K–pretreated frozen sections (b). Panel c shows proteinase K–pretreated negative control specimen without applying antigen solution. Inhibition of endogenous peroxidase and endogenous biotin activities is shown. Bar indicates 50 μm.

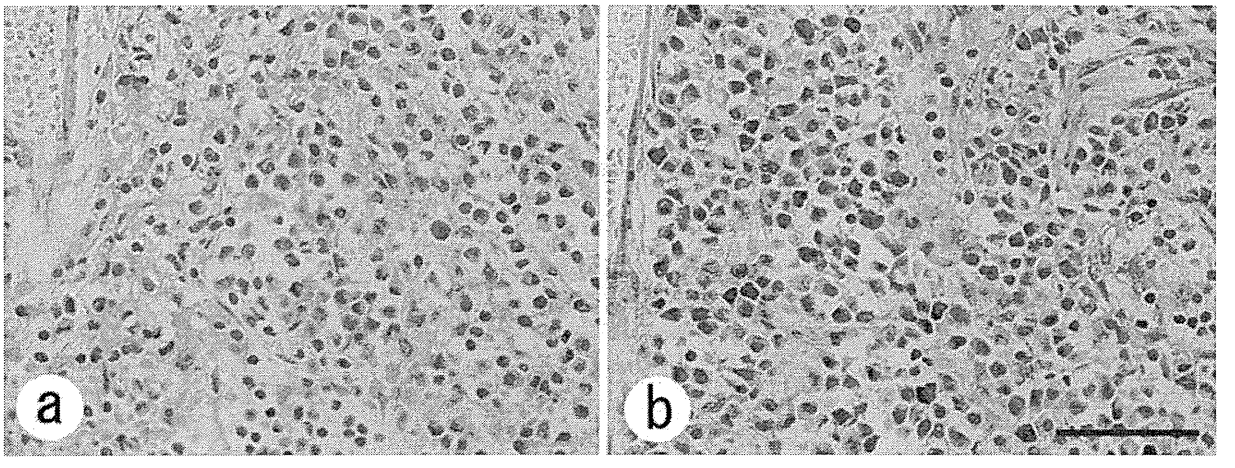

Figure 4. Evaluation of the suitable concentration of biotinylated protein solutions in the enzyme-labeled antigen method. Purified biotinylated Arg-hgp was diluted at the concentration of 10 μg/mL (a) and 50 μg/mL (b) and applied to proteinase K–pretreated frozen sections of the axillary lymph node of rat immunized with Ag53-positive *Porphyromonas gingivalis*. Signals are very weak when the concentration is low (10 μg/mL). The concentration at 50 μg/mL is suitable to get strong signals and low background. Bar indicates 50 μm.

plasma cells were distributed mainly in the medulla of the nodes. Plasma cells producing antibodies to Arg-pro were demonstrated in the popliteal lymph node of one rat immunized with Ag53-negative bacteria. Antibodies to Ag53 were detected only in the lymph nodes of Ag53-immunized rats (n=3). The lymph nodes in the control rats (n=2) did not react with any labeled antigen.

The results are summarized in Table 2, and representative features are illustrated in Figure 5.

Analysis of 10 Radicular Cyst Lesions

The results of both the AlphaScreen method and the enzyme-labeled antigen method in human cases are summarized in

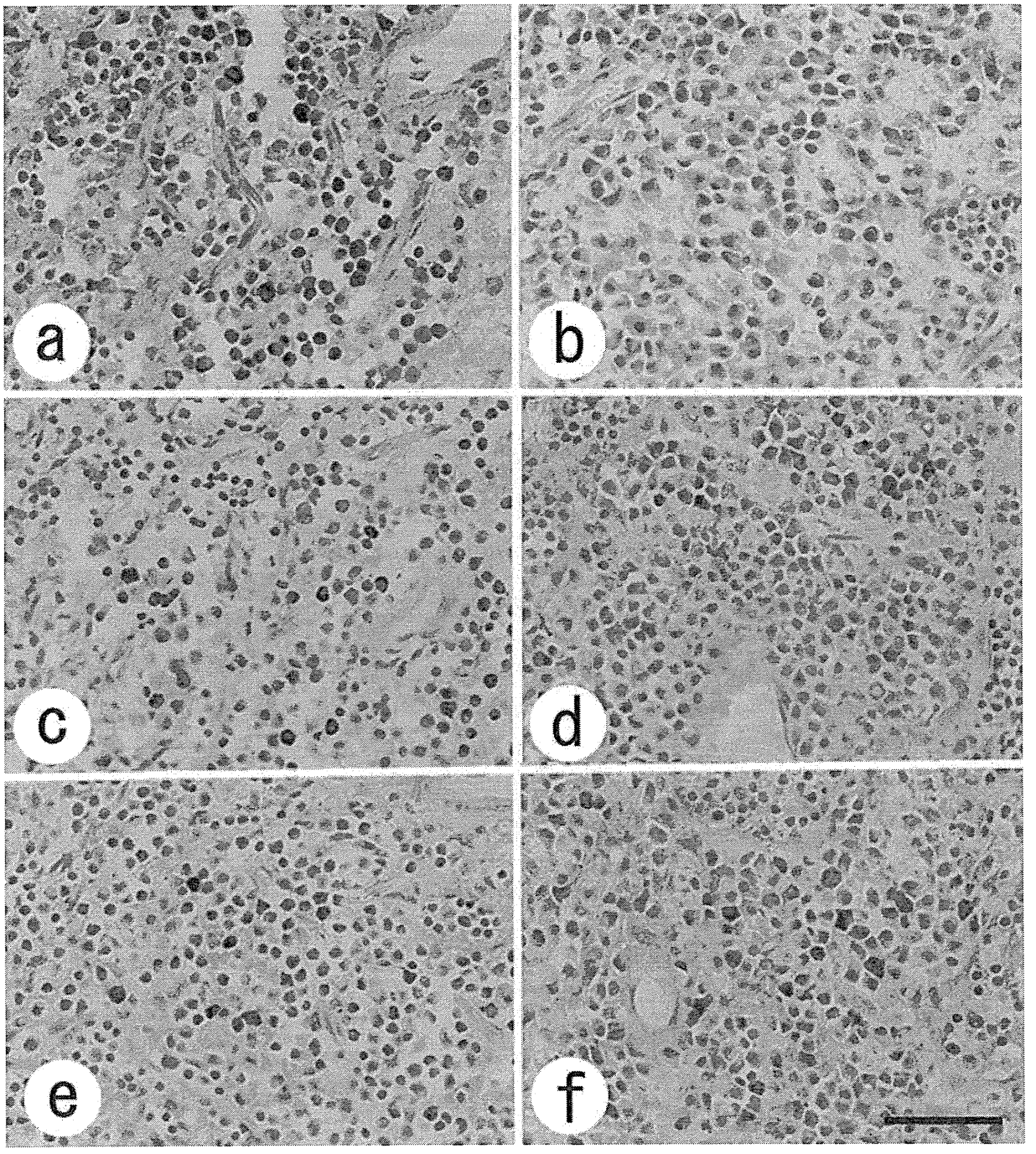

Figure 5. Visualization of plasma cells producing antibodies against *Porphyromonas gingivalis*–related proteins in proteinase K–pretreated frozen sections of rat popliteal lymph nodes with the enzyme-labeled antigen method. Anti-Ag53 antibodies are demonstrated in nodal tissue immunized with Ag53-positive strain (a) but undetectable in tissue immunized with Ag53-negative strain (b). Anti-Arg-hgp antibodies (c, d) and anti-Lys-hgp antibodies (e, f) are seen in a good number of plasma cells in tissues immunized with either the Ag53-positive (left panels: c and e) or Ag53-negative strains (right panels: d and f). Bar indicates 50 μm.

Table 3. Sera and frozen sections were evaluated in all 10 cases, whereas tissue extracts were available in 6.

With the AlphaScreen method, antibodies specific to Arg-hgp and Lys-hgp were demonstrated in the tissue

Table 3. Summary of the AlphaScreen Method and the Enzyme-Labeled Antigen Method in 10 Patients with Radicular Cyst

Case	1		2		3		4		5		6		7		8		9		10	
Age/sex	49M		42M		52M		50M		43M		38F		60F		47M		47F		28F	
Site	UM		UI		UI		UI		UI		LP		LM		LM		LM		UI	
Size (cm)	3.4		1.6		2.2		1.9		1.7		2.1		1.9		2.8		1.4		0.8	
Periodontitis	Moderate		Moderate		Mild		Moderate		Mild		None		None		Moderate		None		None	
Sample	T	S	T	S	T	S	T	S	T	S	T	S	T	S	T	S	T	S	T	S
AlphaScreen method																				
Ag53	1.4	1.7	NE	1.7	1.3	1.7	1.0	**2.1**	NE	1.4	0.9	1.3	NE	1.5	NE	1.4	0.9	1.4	0.8	1.2
Arg-pro	1.1	1.1	NE	1.3	1.1	1.2	0.7	1.3	NE	1.2	1.2	1.2	NE	1.2	NE	1.4	0.8	1.1	0.8	1.1
Arg-hgp	1.1	1.6	NE	1.3	**7.7**	1.6	1.2	**2.5**	NE	1.3	**7.4**	1.7	NE	1.4	NE	**4.2**	1.0	1.1	1.0	1.4
Lys-pro	1.2	1.4	NE	1.4	1.2	1.3	0.8	1.5	NE	1.2	1.0	1.2	NE	1.3	NE	**8.5**	1.5	1.2	1.0	1.2
Lys-hgp	1.2	1.8	NE	1.5	**3.4**	1.8	1.2	**2.5**	NE	1.3	**8.6**	1.7	NE	1.4	NE	**7.0**	1.0	1.3	1.7	1.6
SpaP	1.1	1.2	NE	1.3	1.1	1.3	0.7	1.4	NE	1.2	0.8	1.0	NE	1.3	NE	**4.2**	1.0	1.3	0.9	1.3
Enzyme-labeled antigen method																				
Ag53	–		–		–		NP		–		–		–		NP		–		–	
Arg-pro	–		–		–		NP		–		–		–		NP		–		–	
Arg-hgp	–		–		+		NP		–		+		–		NP		–		–	
Lys-pro	–		–		–		NP		–		–		–		NP		–		–	
Lys-hgp	–		–		–		NP		–		+		–		NP		–		–	
SpaP	–		–		–		NP		–		–		–		NP		–		–	

Site: UM, upper molar; UI, upper incisor; LP, lower premolar; LM, lower molar. Sample: T, tissue extract; S, serum. NE, not examined; NP, no plasma cells seen in frozen sections. AlphaScreen method: Data no less than 2.0 are regarded as positive, represented with bold figures. + indicates positive reaction with the enzyme-labeled antigen method.

extract from two of six cases examined (cases 3 and 6), but the specific antibodies were not elevated in the serum in these two cases. In contrast, specific antibodies were elevated in the serum in two cases (cases 4 and 8): In case 4, low serum titers against Ag53, Arg-hgp, and Lys-hgp were detected, and in case 8, high titers against Arg-hgp, Lys-hgp, Lys-pro, and SpaP were shown. In these two cases, however, plasma cells were scarcely observed in frozen sections of the surgically removed radicular cyst. When the degree of periodontitis was reviewed, these two cases complicated moderate-degree periodontitis. Although cases 1 and 2 also showed moderate-degree periodontitis, all the cases with mild-degree (n=2) or no (n=4) periodontitis were AlphaScreen negative.

On proteinase K–pretreated fixed frozen sections, plasma cells were infiltrated in a total of eight lesions of radicular cyst. Purified biotinylated proteins were used as probes, except for SpaP, for which crude (unpurified) solutions were applied. In cases 3 and 6, positive signals for Arg-hgp were detected by the enzyme-labeled antigen method. The cytoplasm of plasma cells, often clustered beneath the squamous epithelial lining, showed homogeneous positivity. Antibodies against Lys-hgp were also visualized in a small number of plasma cells in case 6. The AlphaScreen titration was very high (more than 7) in these positive cases. No signals were demonstrated in the other sections. Representative features in case 6 are illustrated in Figure 6.

The results of the double immunofluorescence study are illustrated in Figure 7. Inflammatory cells showing cytoplasmic signals positive for Arg-hgp in cases 3 and 6, as well as the cells positive for Lys-hgp in case 6, were labeled for CD138 mainly along the plasma membrane. The plasmacytic nature of the signal-positive cells was thus confirmed. Squamous epithelial cells were also CD138 positive.

When paraffin sections were reviewed, the histological features of cases 3 and 6 were indistinguishable from other cases. All but one (case 8) showed dense infiltration of plasma cells in the cyst wall. In case 4, plasma cells were plentiful in paraffin sections in contrast to frozen sections. Foamy cells were clustered in cases 5 and 10, and neutrophils were rich in case 7.

Absorption Test for Confirming the Specificity of Staining

The positive anti-Ag53 signals in plasma cells of rat lymph nodes were eliminated only with an excess amount of unlabeled Ag53 antigen. The positive signals of anti-Arg-hgp and anti-Lys-hgp reactivities were not eliminated with unlabeled Ag53, Arg-pro, and Lys-pro in both rat and

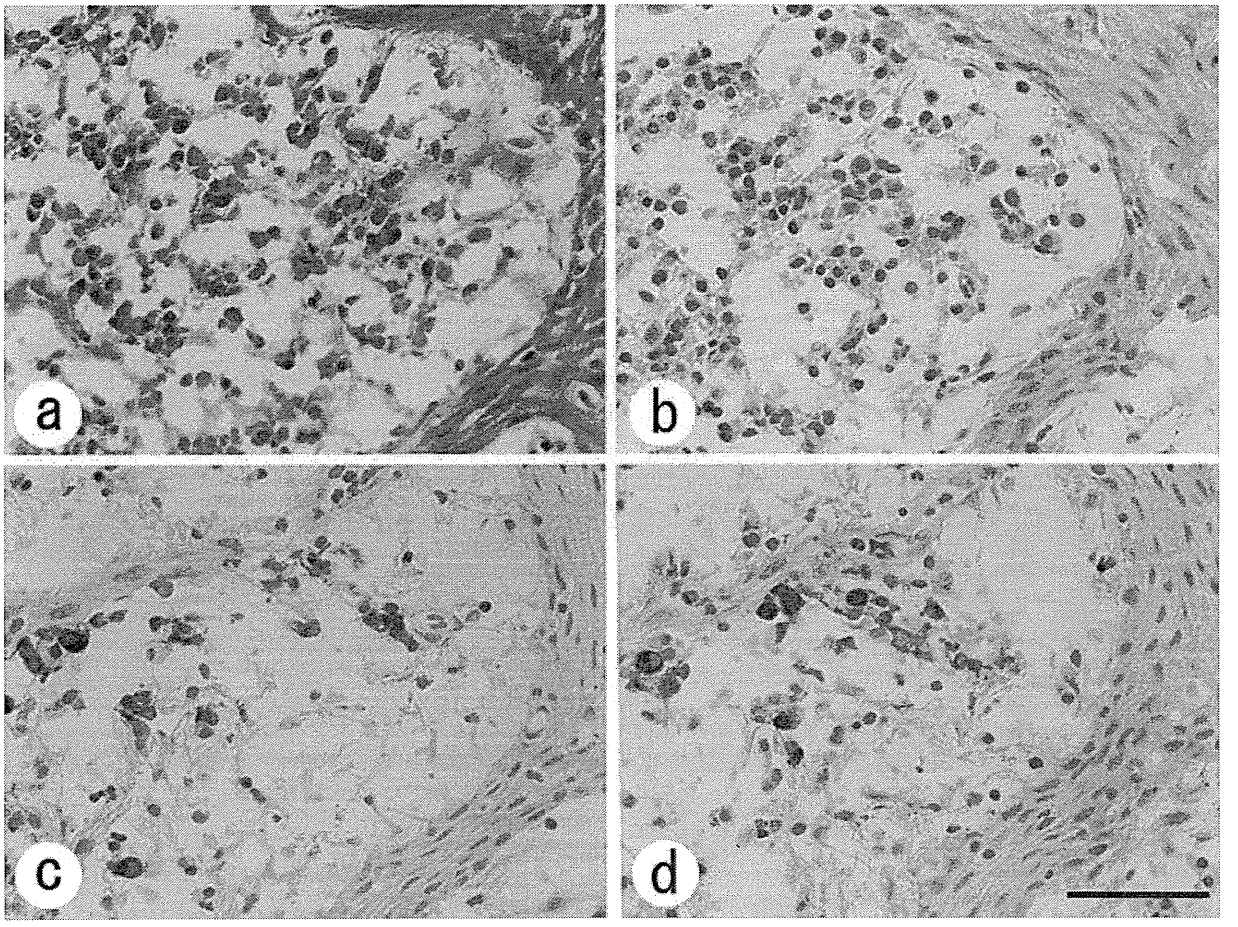

Figure 6. Visualization of plasma cells producing antibodies against *Porphyromonas gingivalis*–related proteins in proteinase K–pretreated frozen sections of radicular cyst (case 6) with the enzyme-labeled antigen method. Plasma cells are clustered beneath the squamous epithelial lining in the gingival cystic lesion (a: hematoxylin and eosin staining). Antibodies against Ag53 (b) are negative in the lesion, whereas antibodies against Arg-hgp (c) and Lys-hgp (d) are localized in the cytoplasm of plasma cells clustered just beneath the squamous epithelial lining. Bar indicates 50 μm.

human tissues. When biotinylated Arg-hgp or Lys-hgp was diluted with unlabeled Arg-hgp or Lys-hgp, a considerable percentage of the positive signals in plasma cells in rat and human tissues disappeared or became significantly weakened, indicating the production of antibodies against the common epitope between Arg-hgp and Lys-hgp (Fig. 8).

In the radicular cyst of case 6 and some lymph nodes of the rat (Fig. 8f), in addition to antibodies directed toward the common epitope, antibodies specific to either Arg-hgp or Lys-hgp were also demonstrated. In some areas of the case 6 lesion, clustered plasma cells were reactive with both biotinylated Arg-hgp and Lys-hgp, and the reactivity was considerably weakened after incubating with unlabeled Arg-hgp or Lys-hgp. In other areas, dispersed plasma cells were reactive with biotinylated Arg-hgp but not with biotinylated Lys-hgp, and the reactivity was weakened with unlabeled Arg-hgp but not with unlabeled Lys-hgp (Fig. 9). The plasma cells in the latter region were considered to produce antibodies against an Arg-hgp-specific epitope. Similarly, antibodies against Lys-hgp-specific epitopes were also recognized in plasma cells in case 6. In the case 3 lesion where anti-Arg-hgp signals were detected without signals against Lys-hgp, anti-Arg-hgp reactivity was abolished with Arg-hgp but not with Lys-hgp, again proving antibody production specific to the epitope unique in Arg-hgp.

Discussion

We documented herein the novel application of the AlphaScreen method and the enzyme-labeled antigen method for demonstrating antibody production against